


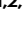




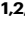




Outcome of SARS-CoV-2 reinfection depends on genetic background in female mice

Received: 19 November 2023

Accepted: 6 November 2024

Published online: 23 November 2024

 Check for updates

Gagandeep Singh ^{1,2,12}, Juan García-Bernalt Diego ^{1,2,12}, Prajakta Warang ^{1,2}, Seok-Chan Park^{1,2}, Lauren A. Chang ^{1,2,3}, Moataz Nouredine^{1,2,3}, Gabriel Laghali^{1,2,4}, Yonina Bykov^{1,2,3}, Matthew Prellberg ^{1,2,3}, Vivian Yan ^{1,2,3}, Sarabjot Singh⁵, Lars Pache ⁶, Sara Cuadrado-Castano ^{1,2,7,8}, Brett Webb⁹, Adolfo García-Sastre ^{1,2,10,11} & Michael Schotsaert ^{1,2,7,8} 

Antigenically distinct SARS-CoV-2 variants increase the reinfection risk for vaccinated and previously exposed population due to antibody neutralization escape. COVID-19 severity depends on many variables, including host immune responses, which differ depending on genetic predisposition. To address this, we perform immune profiling of female mice with different genetic backgrounds –transgenic K18-hACE2 and wild-type 129S1– infected with the severe B.1.351, 30 days after exposure to the milder BA.1 or severe H1N1. Prior BA.1 infection protects against B.1.351-induced morbidity in K18-hACE2 but aggravates disease in 129S1. H1N1 protects against B.1.351-induced morbidity only in 129S1. Enhanced severity in B.1.351 re-infected 129S1 is characterized by an increase of IL-10, IL-1 β , IL-18 and IFN- γ , while in K18-hACE2 the cytokine profile resembles naïve mice undergoing their first viral infection. Enhanced pathology during 129S1 reinfection cannot be attributed to weaker adaptive immune responses to BA.1. Infection with BA.1 causes long-term differential remodeling and transcriptional changes in the bronchioalveolar CD11c⁺ compartment. K18-hACE2 CD11c⁺ cells show a strong antiviral defense expression profile whereas 129S1 CD11c⁺ cells present a more pro-inflammatory response upon restimulation. In conclusion, BA.1 induces cross-reactive adaptive immune responses in K18-hACE2 and 129S1, but reinfection outcome correlates with differential CD11c⁺ cells responses in the alveolar space.

Severe acute respiratory syndrome coronavirus 2 (SARS-CoV-2), the causative agent of the coronavirus disease 2019 (COVID-19) pandemic, has evolved into several variants with different characteristics since it originally started circulating at the end of 2019¹. One of the major

challenges in controlling current SARS-CoV-2 infections is to better understand the risk and underlying mechanisms that allow reinfection by different variants of SARS-CoV-2 which may affect vaccine efficacy and protection provided by natural immunity^{2–5}. Additionally, prior

¹Department of Microbiology, Icahn School of Medicine at Mount Sinai New York, New York, NY, USA. ²Global Health and Emerging Pathogens Institute, Icahn School of Medicine at Mount Sinai New York, New York, NY, USA. ³Graduate School of Biomedical Sciences, Icahn School of Medicine at Mount Sinai, New York, NY, USA. ⁴Department of Pharmaceutics, Ghent University, Ghent, Belgium. ⁵RT-PCR COVID-19 Laboratory, Civil Hospital, Moga, Punjab, India. ⁶NCI Designated Cancer Center, Sanford-Burnham Prebys Medical Discovery Institute, 10901 N Torrey Pines Rd, La Jolla, CA 92037, USA. ⁷Lipschultz Precision Immunology Institute (PrISM), Icahn School of Medicine at Mount Sinai, New York, NY, USA. ⁸Icahn Genomics Institute, Icahn School of Medicine at Mount Sinai, New York, NY, USA. ⁹Department of Veterinary Sciences, University of Wyoming, Laramie, WY, USA. ¹⁰Department of Medicine, Division of Infectious Diseases, Icahn School of Medicine at Mount Sinai New York, New York, NY, USA. ¹¹The Tisch Cancer Institute, Icahn School of Medicine at Mount Sinai New York, New York, NY, USA. ¹²These authors contributed equally: Gagandeep Singh, Juan García-Bernalt Diego.  e-mail: michael.schotsaert@mssm.edu

exposure to other respiratory viruses, such as influenza, soon before a secondary SARS-CoV-2 infection, has also proved to have an impact in COVID-19 severity⁶.

The immune response to SARS-CoV-2 infection is complex and influenced by both viral and host factors, with factors such as viral load, duration of exposure, genetics and the presence of comorbidities proving to be important factors^{7–10}. Reinfection can occur as early as 3 months after the primary infection and it is more likely to be caused by antigenic distant variants that can escape virus neutralization by antibodies^{11,12,13–16}. Still, the correlates of protection and disease outcome from SARS-CoV-2 reinfection or secondary infection are yet to be determined and may involve adaptive as well as innate immune mediators. Understanding the factors that influence the immune response to SARS-CoV-2 infection, reinfection and secondary infection is essential for developing effective therapies and preventive strategies.

Animal models are indispensable for investigating the immunological aspects of COVID-19 and to understand the differential responses elicited by the host towards distinct variants. Wild-type mouse strains are resistant to infection with ancestral SARS-CoV-2 variants due to the low affinity of the viral spike protein to mouse angiotensin-converting enzyme 2 (mACE2), the cellular receptor for SARS-CoV-2 entry. The generation of K18-hACE2 mice, that express human ACE2 (hACE2) under the control of the mouse K18 promoter, helped to overcome this limitation in the experimental setting¹⁷. However, the overexpression of hACE2 in tissues other than the respiratory tract, such as the brain, increases the risk of systemic viral infection with high lethality even at low doses of inoculum¹⁸. SARS-CoV-2 variants that circulated later during the pandemic, with N501Y mutation in their S-protein receptor binding domain (RBD), can infect inbred mice strains such as BALB/c, C57BL6, and 129S1¹⁹. SARS-CoV-1 and SARS-CoV-2 replication was observed in lungs of all three inbred mouse strains with 129S1 mice showing higher susceptibility to infection and morbidity^{19–22}.

Here, we used 129S1 and K18-hACE2 mouse strains to study the outcomes of reinfection and secondary SARS-CoV-2 infection. To study reinfection, we used two different variants of SARS-CoV-2, BA.1 (Omicron) and B.1.351 (Beta), both harboring the N501Y mutation in the RBD of their S-protein. After initial exposure to the mild Omicron BA.1, mice were allowed to recover for 4 weeks and were then reinfected with the B.1.351 variant, at a dose that is lethal for naive K18-hACE2 mice, and which typically causes 10–15% transient body weight loss in naive 129S1 mice. To assess SARS-CoV-2 secondary infection after prior infection with an unrelated pathogen, we performed similar experiments in mice that overcame a primary infection with H1N1 influenza virus (NC99, A/New Caledonia/20/99), a virus that causes severe disease in 129S1 mice and around 10% bodyweight loss in K18-hACE2 mice at the chosen dose. Four weeks after NC99 infection, mice were infected (secondary infection) with B.1.351 (Fig. 1). We observed that prior exposure to BA.1 resulted in protection during reinfection with B.1.351 in K18-hACE2 mice. In contrast, 129S1 mice displayed increased morbidity, higher weight loss and lung damage upon reinfection. NC99 primary infection led to the opposite outcome, with NC99-exposed 129S1 mice showing reduced morbidity after B.1.351 secondary infection and NC99-exposed K18-hACE2 showing similar morbidity and lung viral titers to naive mice exposed to B.1.351. The different disease outcomes after reinfection did not correlate with differences in host adaptive immune responses induced after primary infection, as addressed by serology and T cell immunity. However, BA.1 infection profoundly affected the composition and responsiveness of the alveolar CD11c⁺ cell compartment during both in-vivo and in ex-vivo restimulation experiments, and these altered responses were further dependent on mouse genetic background. Furthermore, this genetic background-related altered responsiveness of alveolar CD11c⁺ cells correlates with the differential outcome of disease during reinfection with B.1.351 infection.

Results

Prior exposure to BA.1 or NC99 has opposite effects in disease severity outcomes of K18-hACE2 and 129S1 mice during B.1.351 reinfection

Heterotypic reinfections with different SARS-CoV-2 variants (reinfection) have been widely reported, especially since the emergence of antigenically drifted Omicron lineages able to escape neutralizing antibodies induced by previous infection or vaccination^{2,4,5}. The outcome of the second infection has shown to be influenced by the antigenic match and quality of host immune responses induced by the first infection, ranging from full protection to partial protection^{2,4,5}. Although less explored, some reports suggest that prior exposure to other respiratory viruses, such as influenza, can have a notable impact on SARS-CoV-2 secondary infection⁶.

Here, we tested whether mice that went through mild Omicron BA.1 infection would be protected from severe morbidity during B.1.351 reinfection. The selection of these two SARS-CoV-2 variants was based on our previous results demonstrating that BA.1 infection is mild and causes no morbidity in mice whereas B.1.351 infection can cause more severe morbidity in mouse models and is lethal in the K18-hACE2 mice model¹⁸. Thus, while this infection regime contradicted chronological emergence of the variants, it allowed us to evaluate protection against severe infection conferred by mild disease-causing variant. Additionally, to assess if the effect of BA.1 primary infection in B.1.351 infection severity was virus-specific or a could be provided by a different respiratory infection, 129S1 and K18-hACE2 mice were challenged with 100 PFU of H1N1 influenza virus (NC99, A/New Caledonia/20/99). NC99 infection causes severe disease in 129S1 mice (2 out of 5 mice reached humane endpoint criteria due to NC99 infection) and causes around 10% bodyweight loss in K18-hACE2 mice. Secondary infection of 129S1 and K18-hACE2 mice was carried out 31 days after first infection with 10⁴ PFU of mild morbidity-causing SARS-CoV-2 Omicron BA.1 variant [Fig. 1].

Focusing on SARS-CoV-2 reinfection, both mouse strains exposed to BA.1 showed a 1.5 log₁₀ reduction in B.1.351 lung virus titers compared to the first time-infected groups [Fig. 2A (ii), B (ii)]. However, we observed contrasting results in daily body weight data, with B.1.351 reinfected K18-hACE2 mice displaying protection while 129S1 mice showed signs of severe morbidity as measured by body weight loss after B.1.351 infection [Fig. 2A (i), B (i)]. Strikingly different B.1.351 disease severity was observed in mice pre-challenged with NC99, with 129S1 mice being the ones protected from severity while K18-hACE2 showed no difference to the Mock:B.1.351 group [Fig. 2A (i), B (i)]. B.1.351 lung viral titers at 4 DPI were reduced to a similar extent in 129S1 mice pre-exposed with either BA.1 or NC99. On the other hand, K18-hACE2 showed mean B.1.351 titers in NC99 pre-exposed mice similar to those of the Mock:B.1.351 group. We then assessed the increased severity observed in BA.1:B.1.351 129S1 mice by histopathological examination of infected lungs. This was done at 4 DPI, the time point that typically coincides with peak lung virus titers in both mouse strains and with peak body weight loss in 129S1 mice. This time point may be too early to observe peak pathology, as this typically comes later than peak virus replication. Nevertheless, Pathological analysis confirmed the higher pathology score for 129S1 compared to K18-hACE2 mice [Fig. 2A (iii), B (iii)]. In both mouse models, B.1.351 infection promoted inflammation and histiocytosis at the alveolar compartment, which was less severe in B.1.351 reinfected mice. B.1.351 infection also caused necrosis in 129S1. Alveolar inflammation and histiocytosis were present in mock infected 129S1 suggesting a distinct basal inflammatory response inherent to the genetic background of these mice. In contrast to the above results, we observed that B.1.351 reinfection in BA.1 infected 129S1 mice results in enhanced peribronchial and perivascular lymphoid hyperplasia [Fig. 2A (iii), (iii)]. Upon closer examination, B.1.351-challenged 129S1 mice showed higher presence of macrophages with eosinophilic cytoplasm; this was true

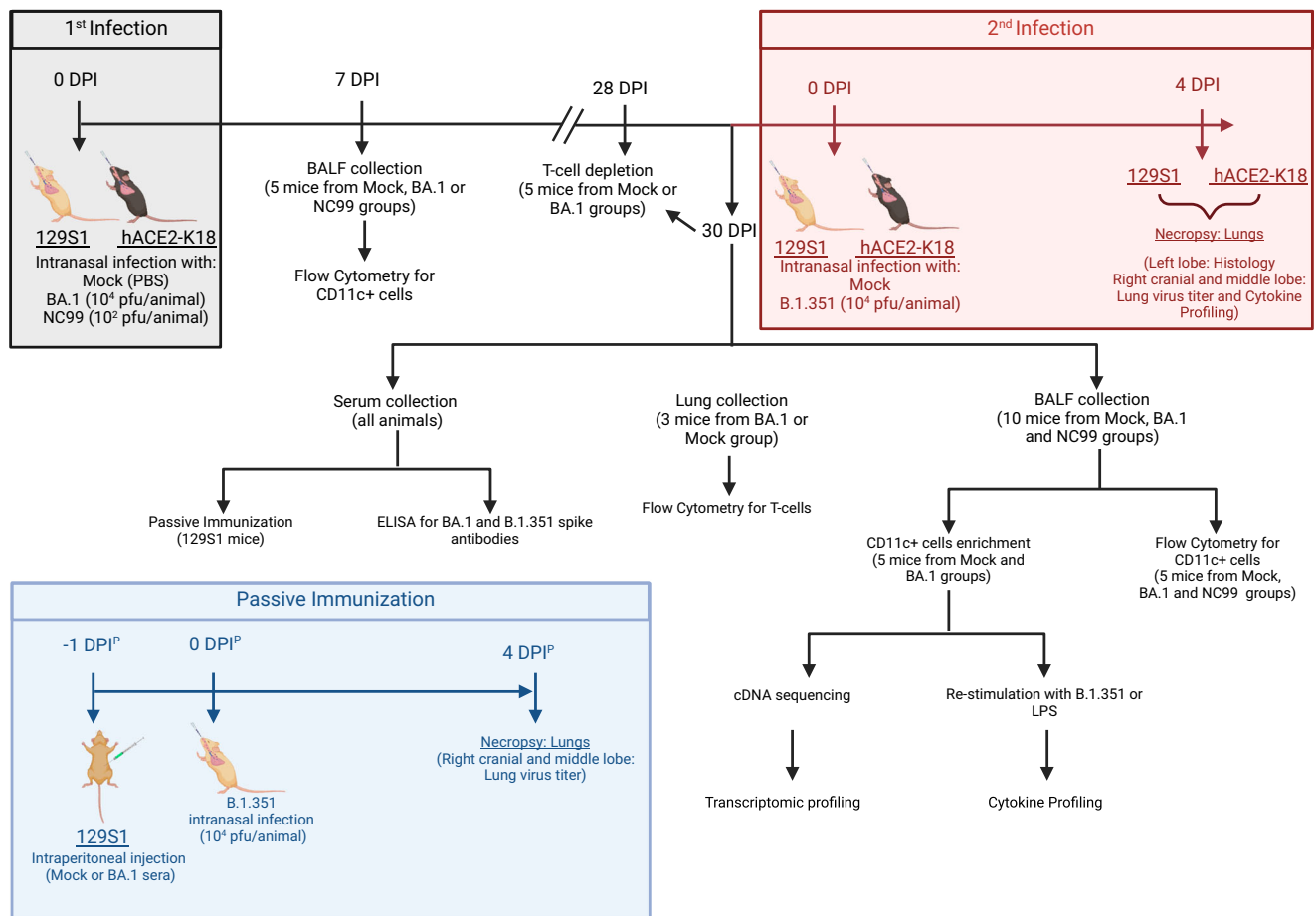


Fig. 1 | Experimental design to assess the impact of reinfection and secondary infection with SARS-CoV-2 in mice with different genetic backgrounds.

Mice were first infected with either Mock (PBS), BA.1 (10⁴ PFU) or NC99 (10² PFU) and allowed to recover for 30 days (1st infection, highlighted in black). 7- and 30-days post infection (DPI), 5 animals from each group were necropsied and bronchioalveolar lavage fluid (BALF) was collected to evaluate CD11c+ populations via flow cytometry. At 30 DPI, BA.1-infected or mock-infected mice ($n = 3$) were euthanized to collect serum, whole lungs and BALF. Whole lungs were used for downstream analysis of T-cell responses by flow cytometry. Bronchioalveolar lavage fluid (BALF; $n = 5$) was the source of CD11c+ cells for isolation, which were further subjected to transcriptome and cytokine/chemokine recall response analysis. Serum collected at 30 DPI was used to assess antibody responses against BA.1 and B.1.351 spike protein and for further passive immunization studies (highlighted in blue). For T-cell depletion experiments, mice were depleted at 28 and 30 DPI (24 h and 72 h

prior to B.1.351 challenge). 31 days after the first infection, mice were challenged with 10⁴ PFU of B.1.351 (2nd infection, highlighted in red). After the 2nd infection, mice's bodyweights were measured daily to assess infection severity. 4 days after B.1.351 challenge (4DPI, highlighted in red), mice were necropsied and lungs were collected for downstream analysis of lung virus titers, lung histopathology and cytokine/chemokine responses. For passive immunization experiments (highlighted in blue), 129S1 mice were intraperitoneal injected with pooled serum from either mock infected or BA.1 infected mice. One day after, mice were infected with B.1.351 (10⁴ PFU). Again, 4 days after B.1.351 infection, mice were necropsied and lungs were collected to assess viral titers, histopathology and cytokine/chemokine responses. The number of mice/group used for the different analyses is mentioned in each figure legend. Created in BioRender. Singh (2022) <https://BioRender.com/a23x374>.

for all 129S1 mice, irrespective of BA.1 prior infection or not, unveiling itself as a distinct hallmark of inflammatory response present at baseline in 129S1 mice [Supplementary Fig. 1A]. Altogether, 129S1 mice and K18-hACE2 mice seem to have different baseline levels of inflammation, as well as composition of the alveolar macrophage compartment.

In addition to the distinct pathology, strain-specific differences were also identified in the cytokine profile displayed by K18-hACE2 and 129S1 mice [Fig. 2C]: B.1.351-only infection of K18-hACE2 mice prompted a Th1-like immune response characterized by high levels of CXCL10, IFN- γ , IL-12p70, GM-CSF, RANTES, TNF- α , MIP-1 α , MCP-3, MCP-1, IL-18 and IL-6. Similar or even higher levels of these Th1-polarizing cytokines/chemokines were found in NC99:B.1.351 group of K18-hACE2 mice, linking this pro-inflammatory Th1 profile to the increased severity observed in this group and the Mock:B.1.351 group when compared to the BA.1:B.1.351 group. On the other hand, levels of these cytokine/chemokines in the BA.1:B.1.351 group were found to

be similar to those in the Mock:Mock K18-hACE2 animals. [Fig. 2C and Supplementary Fig. 1B]. Interestingly, while IL-17A levels were comparable to mock in B.1.351-only infection, we found elevated IL-17A levels in BA.1 and NC99 pre-infected B.1.351 infected K18-hACE2 mice. In contrast to the responses observed in K18-hACE2 mice, B.1.351-only infection elicited both Th1 and Th2 immune response in 129S1 mice [Fig. 2C, Supplementary Fig. 1B]. BA.1 challenged 129S1 mice displayed a raise in the expression of IL-1 β , TNF- α , IL-10, IL-18, IFN- γ , IL-13, IL-5 and IL-10 upon B.1.351 reinfection. 129S1 mice pre-challenged with NC99, showed a similar Th1 cytokine/chemokine profile to the Mock:BA.1, but reduced levels of Th2 cytokines IL-4, IL-5 and IL-13, which could indicate a lower activation of repair mechanisms, due to the lower severity of the secondary infection. In both mouse strains, however, NC99:B.1.351 group is characterized by elevated levels of IL-22, IL-23 and IL-27 when compared both to the Mock:B.1.351 and the BA.1:B.1.351 groups [Fig. 2C, Supplementary Fig. 1B].

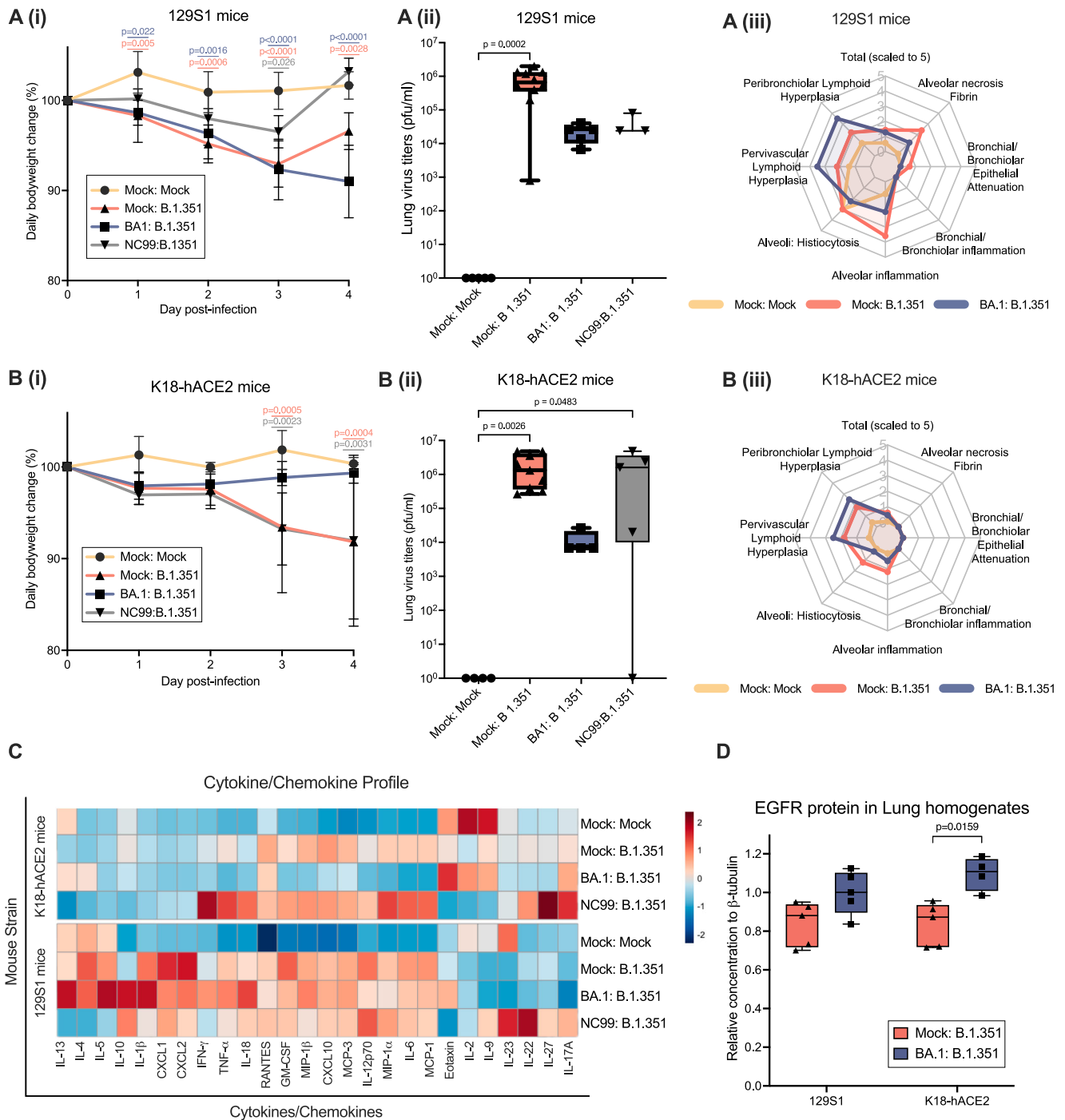


Fig. 2 | Opposite effects of BA.1 or NC99 pre-exposure in B.1.351 disease severity outcomes depending on mouse genetic background. K18-hACE2 or 129S1 mice were infected with B.1.351 31 days after exposure to BA.1 (reinfection, $n = 5$) or NC99 (secondary infection, $n = 5$). A group mock infected twice (Mock:Mock, $n = 5$) and a group mock-infected and challenged 31 days after with B.1.351 (Mock:B.1.351, $n = 10$) were also included. Samples from every mice were used for every analysis unless otherwise specified. **A (i):** Mean \pm SD weight change in 129S1 mice after mock-challenge or challenge with 10^4 PFU of B.1.351. Statistical analysis: Kruskal–Wallis test with Dunnett’s multiple comparisons test to the Mock:Mock group. **A (ii):** Infectious virus titers in the lungs of mock, BA.1 ($n = 5$) or NC99 pre-infected ($n = 3$) 129S1 mice inoculated with 10^4 PFU of B.1.351. Representation: Box-plot with median as center, 25th to 75th percentile-bound box and whiskers representing maximum and minimum values. Statistical analysis: Ordinary two-way ANOVA with Dunnett’s multiple comparisons test to the Mock:Mock group. **A (iii):** Histopathological scores from mock or BA.1 pre-infected 129S1 mice inoculated with mock or

10^4 PFU of B.1.351 ($n = 5$, per group). **B (i):** Mean \pm SD weight change in K18-hACE2 mice after mock-challenge or challenge with 10^4 PFU of B.1.351. Statistical analysis: see **A (i)**. **B (ii):** Infectious virus titer in lungs of mock or BA.1 or NC99 pre-infected K18-hACE2 mice inoculated with mock or 10^4 PFU of B.1.351. Representation and statistical analysis: see **A (ii)**. **B (iii):** Histopathological scores from mock or BA.1 pre-infected K18-hACE2 mice inoculated with mock or 10^4 PFU of B.1.351 ($n = 5$, per group). **C:** Heatmap of cytokine/chemokine profile of lung homogenates from mock, BA.1 or NC99 pre-infected K18-hACE2 or 129S1 mice inoculated with mock or 10^4 PFU of B.1.351. Z-score calculations from average Net-MFI results are represented. **D:** EGFR protein quantification from lung homogenates from BA.1 pre-infected K18-hACE2 mice inoculated with mock or 10^4 PFU of B.1.351 ($n = 5$) or 129S1 ($n = 5$) mice or mock pre-infected [K18-hACE2 ($n = 4$) or 129S1 ($n = 5$)] mice challenged with 10^4 PFU of B.1.351. Representation: see **A (ii)**. Statistical analysis: Two-tailed Mann–Whitney T-test. Statistical significance is represented as exact p -value. Source data are provided as a Source Data file.

The overexpression of Epidermal Growth Factor Receptor (EGFR) and associated signaling pathways has also been reported to correlate with severe disease and enhanced fibrosis during SARS-CoV infection²³. To determine whether enhanced EGFR expression levels were associated with the pathological cases observed in our reinfection mice models, we analyzed the EGFR protein content in lung homogenates from B.1.351 re-infected and first-time infected mice. In both K18-hACE2 and 129S1 mice, reinfection with B.1.351 led to higher levels of EGFR when compared to mice that were infected in the absence of prior virus exposure [Fig. 2D].

129S1 and K18-hACE2 mice exhibit similar adaptive immune responses against BA.1 infection

Next, we investigated whether the genetic background could affect the adaptive immune responses against infection in our experimental setup. After BA.1 infection, humoral and cellular adaptive responses were assessed by ELISA and flow cytometry after, respectively. ELISA results revealed that BA.1 infection elicited comparable antibody responses against BA.1- and B.1.351- spike protein in both 129S1 and K18-hACE2 genetic backgrounds [Fig. 3A (i) and (ii); Supplementary Fig. 2]. We then postulated that differences in morbidity and pathology might be due to the induction of cross-reactive but non-neutralizing anti-SARS-CoV-2 antibodies in 129S1 mice. Therefore, we repeated the B.1.351 infection experiment in naïve 129S1 or mice after passive transfer of serum from BA.1 or mock-infected animals [Fig. 1]. Interestingly, passive transfer of anti-BA.1 immune serum into naïve 129S1 mice conferred protection against severe disease [Fig. 3B (i)] after B.1.351 infection, presenting similar $-1.5 \log_{10}$ reduction in lungs viral titers as in BA.1 pre-infected mice [Fig. 3B (ii)].

Then we focused on the T-cell component of the adaptive immune response. First, we performed a flow cytometry analysis of the T cell compartment, which revealed that mice from both genetic backgrounds had similar proportions of SARS-CoV-2 spike-specific CD8+ T-cells and tissue resident memory CD8+ T-cells (TRMs, CD44+ CD103+ CD69+ tetramer+) in total digested lungs [Fig. 3C (i) and (ii)]. To further establish the role of T-cell mediated adaptive immune responses in the increased severity of B.1.351 reinfection 129S1 mice, we performed CD4+/CD8+ T-cell depletion in naïve and BA.1 pre-challenged mice by injecting T-cell-depleting antibodies 72 h and 24 h prior to B.1.351 challenge [CD8+ T cells were depleted until 4 DPI, CD4+ T cells could be detected again by that time point, see methods section and Supplementary Fig. 2B]. When T-cells were depleted in 129S1 mice, BA.1:B.1.351 reinfected animals showed similar lung viral titers to those of Mock:B.1.351 groups, suggesting a role for T-cells in lung viral control in 129S1 mice [Fig. 3D]. Additionally, cytokine profiling revealed that T-cell depletion of BA.1:B.1.351 mice led to a mitigation of the Type 2 cytokine/chemokine profile observed in non-depleted animals, while relevant Th1 cytokines/chemokines such as TNF- α , RANTES or CXCL-2 remained elevated. Additionally, other proinflammatory IL-2 and IL-6 cytokines presented elevated levels in T-cell depleted BA.1:B.1.351 reinfected mice [Fig. 3E]. In all, these results suggest that T-cell adaptive responses are correlated with the Type 2 immune skewing observed in 129S1 mice during reinfection but also play a protective role in controlling viral titers and inflammation during reinfection, probably acting against the increased severity observed in immunocompetent BA.1:B.1.351 reinfected 129S1 mice. Therefore, other components of the immune response are likely to contribute to the differential pathology observed between 129S1 and K18-hACE2 mice.

BA.1 challenge leads to a substantial alveolar compartment remodeling, with CD11c+ cells that react differently during ex vivo restimulation depending on mouse genetic background and prior exposure to BA.1 virus

Unresolved inflammation at the alveolar space seems to be the major driver of morbidity and differential pathology observed between 129S1

and K18-hACE2 mice. Our lung histological analysis showed that 129S1 mice harbored macrophages with abundant eosinophilic cytoplasm in the alveolar spaces of the lungs, those been distinct and absent in K18-hACE2 mice [supplementary Fig. 1]. Moreover, exposure to respiratory viruses can result in remodeling of the lung myeloid compartment and priming of the alveolar macrophages to respond differently to new innate stimuli^{24–26}.

Therefore, we next focused on investigating whether alveolar macrophages are pivotal to the distinct immune responses observed in 129S1 and K18-hACE2 mice. To this end, first we characterized the CD11c+ compartment in BALF by flow cytometry of mice challenged with BA.1, NC99 or mock-challenged, at an early timepoint after infection (7 DPI) as well as a later timepoint (30 DPI).

Overall CD11c+ cells were slightly reduced in NC99 challenged 129S1 mice by 7 DPI while they were slightly increased in K18-hACE2 mice at the same timepoint, but no differences were observed between the Mock and BA.1 infected groups. Strikingly, at 30 DPI, BA.1-challenged K18-hACE2 mice presented significantly more CD11c+ cells when compared to the other two groups, while no significant differences were found in 129S1 mice [Fig. 4A, B]. FlowSOM and UMAP analysis of the CD11c+ compartment reveal that the highest expression of CD11c+ was by alveolar macrophages, that were mostly MHII+, with some MHCII- alveolar macrophages are also present, particularly in 129S1 mock mice. MHCII+ alveolar macrophages were the most abundant CD11c+ cell subpopulation in mock groups, representing between 83–93% the cells in 129S1 mice and 60–76% in K18-hACE2. NC99 infection led to an extreme reduction of MHCII+ alveolar macrophages at 7 DPI in both strains (13.1% in 129S1 and 16.4% in K18-hACE2) and a strong recruitment of inflammatory monocytes to replace the macrophages lost. While BA.1 led to some alveolar macrophage loss, this was very limited compared to NC99 mice. Infiltrating inflammatory monocytes were more abundant in K18-hACE2 than 129S1 at 7 DPI (16.3% and 9.45%, respectively), a difference that increased even more by 30 DPI (20.3% and 1.87%, respectively). Other CD11c+ immune cells, including different subpopulations of dendritic cells and a third subpopulation of alveolar macrophages (which we call B220- alveolar macrophages in Fig. 4 as they have lower B220 baseline expression levels compared to other alveolar macrophage subsets) revealed less remarkable differences in BA.1 challenged mice, and increased levels were mainly associated with NC99 challenge [Fig. 4C–G]. Overall, there is a significant remodeling of the CD11c+ alveolar compartment due to BA.1 or NC99 primary challenge, which could have an important impact on B.1.351 reinfection or secondary infection.

As some relevant differences were found in the CD11c+ compartment, that were maintained even through 30 DPI, we aimed to characterize the responsiveness of CD11c+ ex-vivo to different stimuli. To this end, CD11c+ cells were isolated from the BALF of infected mice 30 days after exposure to BA.1 [Fig. 1]. Pooled CD11c+ cells were next stimulated ex vivo with either 10^7 PFU of live SARS-CoV-2 B.1.351 variant, 10 ng/mL of LPS or mock stimulated. Downstream analysis of cytokine/chemokine responses from CD11c+ cells revealed differences associated to genetic background both at baseline as well as after BA.1 exposure [Fig. 5A].

The levels of TNF- α were high in mock groups of both models, being almost 2 times higher in 129S1 mice than in K18-hACE2 mice. These TNF- α levels in both mouse models dropped for mock-challenged mice when stimulated with the B.1.351 variant, with the 129S1 group showing -10 times reduction, while K18-hACE2 only show -2 times reduction. When comparing mock-infected groups to BA.1-infected groups, TNF- α levels were lower in BA.1-infected mice, with a -5 times reduction in K18-hACE2 and -2 times reduction in 129S1 [Fig. 5A, supplementary fig. 5]. The levels of MIP-2 α were also elevated and were similar in the mock groups of both models (-1500 pg/mL), however only in 129S1 these levels dropped -5 -fold when stimulated

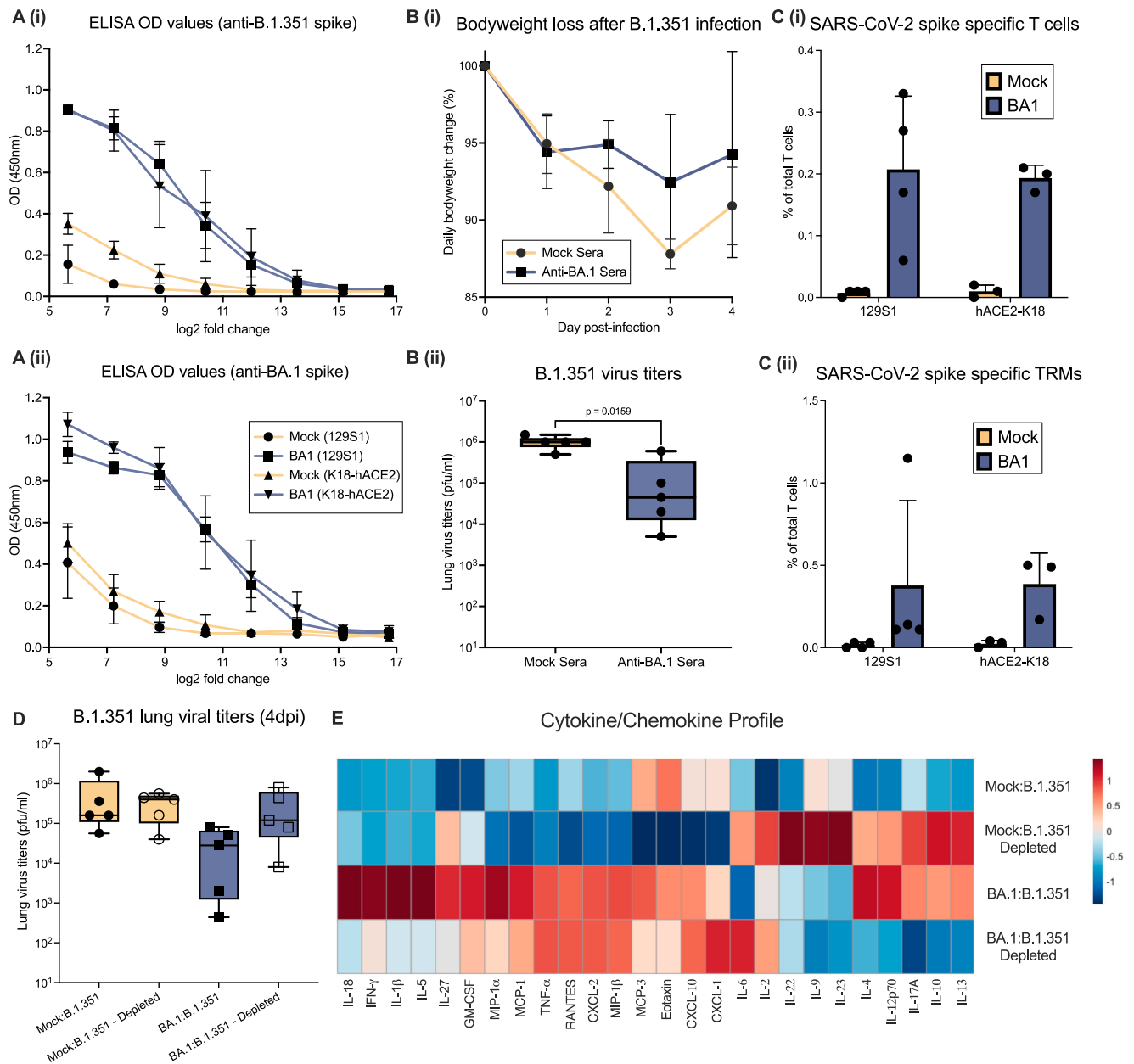


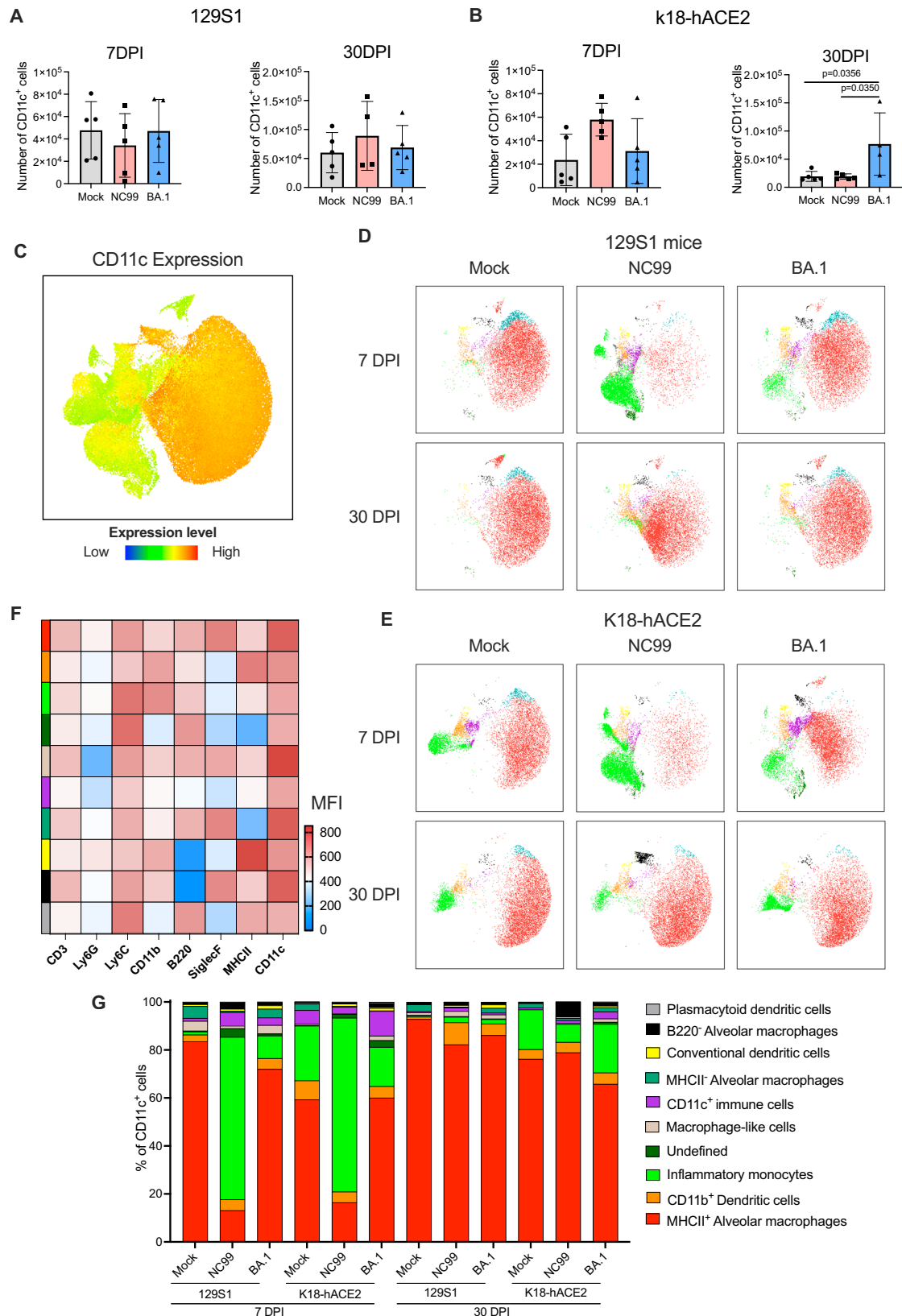
Fig. 3 | Differences in adaptive immune responses upon BA.1 infection do not explain differences in re-infection outcomes. **A** Line graph showing ELISA results in transformed \log_2 fold dilutions (x-axis) of 30 DPI serum from K18-hACE2 ($n = 4$) and 129S1 ($n = 5$) versus mean \pm SD OD values at 450 nm (y-axis) against B.1.351 spike (i) or BA.1 spike (ii) protein. **B** (i): Mean \pm SD weight change in 129S1 mice inoculated with 10^4 PFU of B.1.351 after passive immunization with either mock ($n = 5$) or anti-BA.1 serum ($n = 5$). **B** (ii): Infectious virus titers in lungs from passive immunized 129S1 mice with either mock ($n = 5$) or anti-BA.1 serum ($n = 5$) 4 DPI after B.1.351 inoculation. Representation: Box-plot with median as center, 25th to 75th percentile-bound box and whiskers representing maximum and minimum values. Statistical analysis: Two-tailed Mann–Whitney T-test. **C** (i): Spike-specific T-cells as percentage (mean \pm SD) of total T cells in murine lungs at 30 DPI after BA.1 or mock

challenge (129S1 mice $n = 4$ per group, K18-hACE2 mice $n = 3$ per group). **C** (ii): Spike-specific tissue resident memory T-cells as percentage (mean \pm SD) of total T cells in murine lungs at 30 DPI after BA.1 or mock challenge (129S1 mice $n = 4$ per group, K18-hACE2 mice $n = 3$ per group). **D**: B.1.351 lung viral titers 4 DPI in 129S1 mice pre-exposed or not to BA.1, either T-cell depleted or immunocompetent ($n = 5$, per group). Representation: see **B**(ii), **E** Heatmap graph of cytokine/chemokine profile of lung homogenates from mock or BA.1 pre-infected 129S1 mice, either T-cell depleted or not, inoculated with either 10^4 PFU of B.1.351. Z-score calculations from Net-MFI results are represented in the heatmap ($n = 5$, per group). Mann–Whitney t-test was used to determine statistical significance of the results, where exact p -values are presented. Source data are provided as a Source Data file.

with B.1.351 variant [supplementary data]. Conversely, in BA.1-infected groups, the level of MIP-2 α was lower in the K18-hACE2 group compared to the K18-hACE2 mock infected group as well as the 129S1 BA.1 infected group [Fig. 4A, Supplementary Fig. 5]. Surprisingly, we observed that IFN- γ , IL-17A, IL-22 was only induced by LPS stimulation in BA.1 infected K18-hACE2. IL-13 and IL-18 were high in 129S1 mock group and were upregulated in the BA.1 infected group. However, these levels were reduced with B.1.351 stimulation, whereas LPS

boosted production in all groups. BA.1 infected 129S1 CD11c $^+$ BALF cells also showed higher levels of Eotaxin when compared to other groups [Fig. 5A, Supplementary Data].

Transcriptome profiling of CD11c $^+$ cells from BALFs also revealed differential gene expression between both mouse strains. Gene enrichment analysis assigned cell subsets from both BA.1 infected mouse strains as M1 macrophages. Other 129S1 cell subsets were classified more similar to RAW 264 and osteoblasts whereas cells from K18-



hACE2 showed more similarity to CD8⁺ T-cells and B220⁺ B-cells [Supplementary Fig. 6]. GO (Gene ontology analysis) for biological processes also showed contrasting results between both mouse strains, where cells from K18-hACE2 showed positive regulation of the immune response, and 129S1 cells showed negative regulation of the immune response (Supplementary Fig. 6).

Even without infection, CD11c⁺ cells from K18-hACE2 and 129S1 presented markedly different gene expression profiles. While some relevant genes including *Irf3*, *Sting1*, *Mavs*, *Cwcl5*, *Rigl1*, *Tlr7*, *Tlr8*, *Cd2*, *Mif*, *Iho1*, *Sod1*, *Tuba1c* or *Zfas1* had similar levels in cells from both mouse strains; several relevant genes were highly expressed in CD11c⁺ cells from K18-hACE2 mice, but not in 129S1 mice (for example *Alcam*,

Fig. 4 | CD11c+ alveolar compartment is extensively remodeled after BA.1 and NC99 infection. Early (7 DPI) and late (30 DPI) timepoints after NC99 or BA.1 infection reveal profound changes in the CD11c+ subpopulations of BALF. **A** Total number of CD11c+ cells (mean \pm SD) in BALF collected from 129S1 mice 7- and 30-days post infection with Mock ($n = 5$ per timepoint), NC99 ($n = 5$ at 7DPI, $n = 4$ at 30DPI) or BA.1 ($n = 5$ per timepoint). **B** Total number of CD11c+ cells (mean \pm SD) in BALF collected from K18-hACE2 mice 7DPI and 30 DPI with Mock ($n = 5$ per timepoint), NC99 ($n = 5$ per timepoint) or BA.1 ($n = 5$ at 7DPI, $n = 30$ at 30DPI). Statistical analysis by ordinary one-way ANOVA with Dunnett's multiple comparison. **C–G** Dimensionality reduction analysis performed by Uniform Manifold Approximation and Projection with a Nearest-Neighbours clustering algorithm combined with FlowSOM cluster visualization algorithm. Data from mice in the sample group

was combined and randomly downsampled to a total of 10,000 events per group prior to the analysis dimensionality reduction analysis. **C** Expression levels of CD11c+. Higher expression levels indicated by red colors; lower expression levels indicated by green colors. **D** CD11c+ subpopulation clusters in BALF collected from 129S1 animals either mock-, NC99- or BA.1-challenged, 7 or 30 DPI. **E** CD11c+ subpopulation clusters in BALF collected from K18-hACE2 animals either mock-, NC99- or BA.1-challenged, 7 or 30 DPI. **F** Heatmap of the expression of CD3, Ly6G, Ly6C, CD11b, B220, SiglecF, MHCII and CD11c markers in the different populations. **G** Stack bar plot with the frequencies of the different CD11c+ populations in 129S1 and K18-hACE2 mice, depending on the infection and the day of collection of the BALF. Experiments were performed with 5 or 4 mice per group and per timepoint. Source data are provided as a Source Data file.

Ccl4, *Wdr83*, *Bpifa1*, *Cd44*, *Lima1*, *Xbp1* or *Cd74*) or viceversa (for example *Lyz2*, *Ccl6*, *Ly6e*, *Cxcr4*, *Tnf*, *Lrrfip2*, *Btg1*, *Ly9a*, *Cd52*, *Bcl2a1a*, *Cxcr4*, *Cd22*, *Tnfrsf1a* or *Cxcl16*) [Fig. 5B]. The expression of these genes and many others was greatly altered in CD11c+ cells obtained from BA.1-challenged mice. Infection with BA.1 led to the upregulation of over 6500 genes and downregulation of 4600 genes in K18-hACE2 mice and over 3900 were upregulated and 4900 downregulated in 129S1 mice (differentially expressed genes with a $\log_2(\text{Fold change}) > |1|$). Among the top 100 genes most upregulated by BA.1 in K18-hACE2 CD11c+ cells, the most abundant were genes involved in the recruitment, activation and reprogramming of macrophages, including *Lyz2*, *Ccl6*, *Cyba*, *H2-Aa*, *Cd68*, *Ucp2*. Genes involved in other immunological processes and signaling pathways could also be found, such as *Ear2*, which is involved in immunological tolerance; genes related to the NF-kappa-B signaling pathway, like *Ubb*, *Ear1*; wound healing and repair, including *Plet1* or genes involved in type I interferon antiviral response, including *Vamp8*. On the other hand, the top 50 genes more upregulated by BA.1 in 129S1 CD11c+ cells involved a distinct set of pathways from K18-hACE2 cells, including genes involved in inflammatory responses, such as *Chil4* or *Rnase2a*; antibacterial genes, including *Lyz1*; genes regulating chromatin accessibility including *H3f3c* and *Bicral*, chemotactic genes for eosinophils and T-cells like *Ccl24*, the M2 macrophage marker *Arg1* [Fig. 5B]. While this analysis provided interesting information, the expression of most of these genes was upregulated in cells from both mice strains. More revealing was the analysis of genes highly upregulated due to BA.1 infection in cells from one mouse strain, that were downregulated in cells from the other. Focusing on macrophage-related genes, *cd68*, a pan-macrophage marker that has been shown to be upregulated in M1 macrophages when compared to M2, was upregulated in cells from K18-hACE2 mice and downregulated in the ones from 129S1 mice, while *Arg1* had the opposite profile: highly upregulated in 129S1 mice while downregulated in K18-hACE2. This gene profile highlights the differential polarization of macrophages in response to BA.1 in the two mouse strains: M1 in K18-hACE2 and M2 in 129S1. Other highly upregulated genes in K18-hACE2 mice include T-cell marker *cd52* or monocyte-activation marker *Cd300c*. On the other hand, genes highly upregulated in 129S1 mice and downregulated in K18-hACE2 mice included eosinophil-related genes such as the chemoattractant *Ccl24* or the eosinophil produced *Rnase2*. This set of genes also included histone and DNA-accessibility related genes, such as *Bicral*, *H2ac13*, *H2ac7* and *H2bc24* [Fig. 5C]. These gene signatures suggest epigenetic changes after virus infection that have been suggested to be associated with virus-induced trained immunity. The complete list of Top 100 upregulated and downregulated genes in both strains can be found in the source data associated with Fig. 5.

In conclusion, different transcriptomic and cytokine responses are observed in CD11c+ alveolar cells upon restimulation depending on mouse genetic background and prior virus exposure. Our work describes a method to explore genetic drivers of protection or disease during SARS-CoV-2 infection in the context of reinfection and secondary infection.

Discussion

Rapid evolution of SARS-CoV-2 into antigenically different variants poses a greater risk of reinfection with new variants. The disease severity during reinfection depends on several factors such as antigenic distance of the variants, age, sex, comorbidities, and risk of high exposure¹. Here, we used female K18-hACE2 and 129S1 mice, two mouse strains that we have previously shown to be suitable for SARS-CoV-2 studies, to evaluate the protection and immune response after reinfection with a severe variant¹⁹. As a comparison, we also evaluate the immune response to a severe SARS-CoV-2 variant as a secondary infection after a primary infection with H1N1, an unrelated respiratory virus that can also cause severe disease. Some reports also correlate prior influenza infection with severe COVID-19 outcomes in humans, but mechanistic insights are still lacking⁶.

129S1 and K18-hACE2 strains have several differences between quantitative trait loci (QTLs) which can result in different phenotypes under certain conditions^{27–30}. 129S1 mice are known to display more airway responsiveness, more airway cellular infiltration and high IL-4 levels after inhaled ovalbumin compared to the C57BL/6J strain which is of a similar genetic background to the K18-hACE2 mice³¹. 129S1 mice also have been shown to express higher levels of guanylate binding proteins (GBPs) compared to C57BL/6J when stimulated with different antigens³². In humans and mice, GBPs promote inflammation and restrict the replication of intracellular pathogens^{32–35}. One of the main differences between the two strains is that K18-hACE2 can be infected with any SARS-CoV2 variant, 129S1 can only be efficiently infected with variants having mutations associated with mouse-adaption like the N501Y mutation in spike (S) protein, which is also required for infection in wild type mice. Keeping this in mind, we use BA.1 and B.1.351 variants, both of which harbor the N501Y mutation in the S-protein¹⁹. Both variants are also antigenically different with only 93.30% similarity in the receptor binding domain (RBD) of the S-protein³⁶. We hypothesized that prior BA.1 infection would be mild and induce cross-reactive immune responses that are protective during reinfection with a more virulent and antigenically drifted SARS-CoV-2 virus (B.1.351). Although B.1.351 reinfection after BA.1 exposure may not occur in real life, as the B.1.351 circulated in the human population before the appearance of the SARS-CoV-2 omicron lineage that includes BA.1, we chose to continue with this experimental setup to provide proof of principle that a mild infection (BA.1) followed by a severe infection (B.1.351) may have different outcomes based on genetic background¹⁸.

Results highlighted that BA.1 infection was able to reduce the viral load during reinfection in both mouse strains, however, the morbidity, cytokine profile, and histopathology scoring upon reinfection were different based on genetic background. In K18-hACE2, prior BA.1 infection provided protection against morbidity and a cytokine profile that reflects milder disease severity. Whereas in 129S1, prior BA.1 infection exacerbated the outcome, with a cytokine profile that is somewhat similar to what is described for severe COVID-19 infection in humans with enhanced levels of IL-10, IL-18 and IFN- γ suggesting dysregulation of cytokines after BA.1 infection^{37–42}. Strikingly, prior NC99 infection, led to opposite results upon secondary infection with

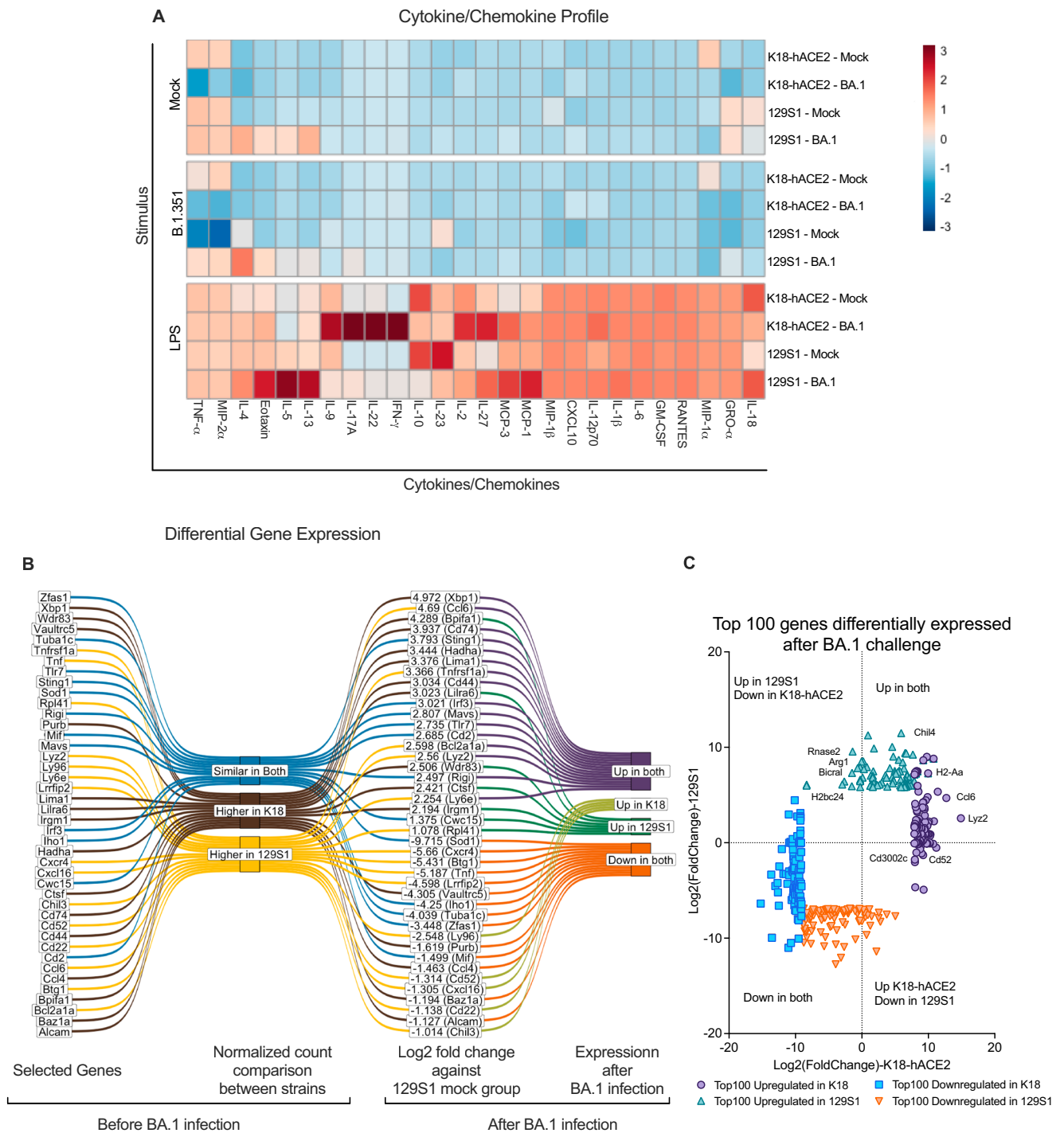


Fig. 5 | CD11c+ cells react differently during ex vivo restimulation depending on mouse genetic background and prior exposure to BA.1 virus. BA.1 inoculated K18-hACE2 ($n = 8$) or 129S1 ($n = 9$) mice were euthanized after 30 DPI, Lungs ($n = 4$ or 3) or BALF ($n = 5$) were collected. CD11c+ cells were enriched from the BALF and used for trained immunity experiment. **A** Heatmap graph of the cytokine/chemokine profile of CD11c+ BALF cells either stimulated with mock media (1X RPMI, upper), Beta (10^4 PFU of B.1.351, middle), or LPS (lower) after 48 h. **B** Results from

the long-read-RNAseq analysis from CD11c+ BALF cells isolated from mice at 30 days post-infection. Sankey diagram selected gene with their relative gene expression in mock groups and their relative change after BA.1 infection in each strain. **C** Top 100 up and down regulated genes by BA.1 infection in CD11c+ cells from 129S1 and K18-hACE2 mice represented as Log2(Fold change). Source data are provided as a Source Data file.

B.1.351, with 129S1 mice being more protected than K18-hACE2. In the case of influenza infection, it is well established that susceptibility of different substrains of 129 mice is significantly higher compared to C57/BL6⁴³, which could have an effect in the phenotype observed upon SARS-CoV-2 reinfection.

Lung pathology was assessed at 4 DPI, which is expected to be too early for peak pathology. This is a limitation of this study since the

difference in lung pathology at a later time point can be due to different degrees of repair after lung tissue injury upon infection, which can vary due to genetic background differences as well. Whereas controlled series of immune events can reduce lung injury and pathology, dysfunctional immune events can lead to fibrosis and scarring resulting in reduced lung function and hence quality of life²³. The persistent damage from infectious viruses such as SARS-CoV and

hepatitis C virus can lead to dysfunctional EGFR levels thus leading to more fibrosis and Type II alveolar cell hyperplasia²³. B.1.351 infection promoted alveolar fibrosis in 129S1 only, which was reduced in mice with prior BA.1 infection. However, EGFR levels in both mouse strains were similar. Interestingly, the B.1.351 reinfected mice from both genetic backgrounds showed higher EGFR levels compared to first-time infected, which was not reflected in the pathological analysis for fibrosis. As reported in humans for some viruses like respiratory syncytial virus, and a problem in the vaccination field, cross-reactive antibodies with low neutralization capacity can increase the risk of severe disease and even death⁴⁴. This seems unlikely in our model since we performed a passive immunization experiment where we obtained similar antibody titers in both strains and passive immunization protects the 129S1 mice, rather than exacerbate disease. T-cells can contribute to immunopathology by causing cellular damage while targeting infected cells, but this is also typically associated with viral load reduction⁴⁵. Alternatively, reduced T-cell numbers can result in less effective viral clearance⁴⁶. Nevertheless, the percentage of virus-induced T-cells were similar in both mouse models, and viral reduction was seen in BA.1-exposed mice in both mouse strains. Moreover, T-cell depletion studies in 129S1 resulted in loss of viral titer reduction in without significant differences in morbidity, further confirming that severity of reinfection was not dependent on lung viral load. This suggests that the distinct outcomes upon reinfection are not because of differences in B- or T-cell responses.

Similarly to the adaptive immune response, the innate immune response can become more responsive after the first infection which involves epigenetic and metabolic alterations after the first infection/insult, referred as 'trained immunity'⁴⁷. With well-guided trained immunity, responses to a second, antigenically similar or different, infection can be protective, whereas with misguided, maladaptive training, responses can be deleterious⁴⁷. To date, trained immunity has been associated primarily to monocyte/macrophage epigenetic and metabolic reprogramming⁴⁸. Other respiratory viruses than SARS-CoV-2, like influenza virus, can cause extensive remodeling of the monocyte and macrophage lung compartment. Therefore, altered responsiveness to reinfection at the tissue level can also be due to alveolar macrophages of embryonic origin being replaced by infiltrating monocytes that became lung resident. Murine alveolar macrophages reprogrammed or replaced by infiltrating monocytes after sublethal influenza infection present altered cytokine and chemokine responses upon subsequent restimulation with LPS⁴⁹. We hypothesized that a similar mechanism could be causing the differences in B.1.351 infection severity we observed in pre-infected animals.

To determine whether the difference is due to differences in lung remodeling of the innate immune cells, we first characterized the CD11c+ cells in BALF after BA.1 infection. We demonstrated most CD11c+ cells (between 70–90%) were mainly alveolar macrophages in both mouse strains. During histological comparison of lungs at baseline (no infection), mouse strain differences could already be observed. 129S1 mice had macrophages with abundant eosinophilic cytoplasm and a higher baseline inflammation compared to K18-hACE2 mice. Abundant eosinophilic cytoplasm of macrophages can be due to eosinophil efferocytosis, which may also have skewed the immune response to Th2 type^{50–53}. Alveolar macrophage death and inflammatory monocyte infiltration caused by BA.1 was not as extensive in either of the mouse strains as the one caused by NC99 infection. Still, remodeling of the CD11c+ compartment was sustained until 30 DPI in BA.1 infected mice, particularly in K18-hACE2 mice, which are the ones protected upon B.1.351 reinfection. Then we enriched CD11c+ cells from the BALF of mock or BA.1 infected mice for ex vivo LPS restimulation. We and others have also observed that prior infection can result in lung remodeling, whereby embryonic alveolar macrophages in the lung are (partially) replaced by infiltrating bone marrow-derived monocytes that upregulate alveolar macrophage markers (CD11c, SiglecF) and

become lung resident²⁵. As such, these recruited myeloid cells can also contribute to altered responses to stimuli during reinfection or ex vivo restimulation. Finally, CD11c in the mouse lung is also expressed by dendritic cells and to some extent by other (lymphoid) cell types. Therefore, isolation of CD11c+ cells from the BALF results in a pool of cells that is rather heterogenous, especially when mice have been exposed before to BA.1 virus. The cytokine/chemokine profile of CD11c+ cells from BA.1-exposed mice revealed that BA.1 infection is modulating the cells differently in both strains, where K18-hACE2 mice cells exhibit a more protective Type 1-like response, while 129S1 cells showed the inflammatory Type 2 response. The CD11c+ cells from the BA.1 pre-infected 129S1 showed persistent production of IL-13 even with mock stimulation, which peaked with LPS stimulation. IL-13 levels were higher in in-vivo B.1.351 infected 129S1 as well.

Persistent levels of IL-13 can cause eosinophilic inflammatory responses resulting in lymphoid hyperplasia, airway fibrosis, and IL-5 and eotaxin production^{54–56}. Our histology data showed a similar pattern, having more lymphoid hyperplasia in 129S1 compared to the K18-hACE2. The RNAseq also confirmed the up-regulation of *Mmp12* (matrix metalloproteinases 12, MMP12) and *Retnla* (resistin-like α , RELM α) gene which can be up-regulated by IL-4 and IL-13. After infection, the macrophage-produced MMP12 protein can suppress the expression of the MMP2, MMP9 and MMP13 collagenolytic proteins which results in diminishing matrix degradation, hence amplified fibrotic responses⁵⁷. The transcriptomic analysis further supported the hypothesis that myeloid compartments are affected by prior BA.1 infection and are different in both mouse strains. RELM α secreted from activated macrophages plays a critical role in modulating type 2 cytokine production^{56–58}. CD11c+ cells from BA.1 infected 129S1 mice upregulated expression of *Arg1* (Arginase 1), while the ones from K18-hACE2 downregulated the expression of this gene after BA.1 challenge. Arginase 1, which is a marker of M2 (immunosuppressive) macrophages, can also be upregulated by IL-4 and IL-13, and is critical for cell proliferation and collagen synthesis^{54,55}. Interestingly, CD11c+ cells from K18-hACE2 mice upregulate *Cd68* (CD68 molecule) after BA.1 challenge, while cells from 129S1 downregulate it. While CD68 is not specific to M1 macrophages, it has been shown to have upregulated expression in M1 macrophages⁵⁹.

BA.1 preinfected 129S1 also showed higher levels of IL-10, which is typically classified as an immunosuppressive and anti-inflammatory cytokine. However, there are several studies where IL-10 enhances the immune cell proliferation and activation resulting in production of pro-inflammatory cytokines^{60–63}. Overexpression of IL-10 alongside with persistent IL-13 expression augments airway fibrosis, mucus metaplasia, and tissue inflammation⁶⁴.

IFN- γ levels upon B.1.351 infection were high in BA.1 pre-infected 129S1, however this was opposite in the CD11c+ cell restimulation experiment, where IFN- γ was only produced in LPS stimulated BA.1 pre-infected K18-hACE2 CD11c+ cells suggesting BA.1 modulated IFN- γ gene expression in K18-hACE2 differently. Even though IFN- γ is a proinflammatory cytokine, it can inhibit IL-13's inflammatory response and eotaxin, and protect against immunopathology which can be helpful during reinfection^{65,66}. The higher IFN- γ level in lung homogenates after B.1.351 infection of BA.1 pre-infected 129S1 can be explained by persistent IL-18 expression by CD11c+ cells after BA.1 infection in conjunction with IL-10 production during B.1.351 infection, as both these cytokines induce IFN- γ production in T-cells and Natural killer (NK) cells⁶⁷. B.1.351 infection in 129S1 also induced significant amounts of another pro-inflammatory cytokine, TNF- α . CD11c+ cells from both strains produced some level of TNF- α even without any stimulation, with 129S1 mice producing more. This is also evident in the transcriptome profile, where 129S1 expressed more *Tnf* gene copies than hACE2-K18. The higher production of TNF- α is further evidenced by higher counts of *Tnfip2* gene (TNF- α induced protein 2) compared to the K18-hACE2. However, the level of TNF- α dropped in

B.1.351 stimulated as well as BA.1 exposed CD11c⁺ cells. This reduction was also observed in the transcriptome profile of 129S1, where *Tnfrsf2* gene expression was downregulated. Several intracellular pathogens can downregulate TNF- α production by macrophages, which can lead to an immunosuppressive condition that favors the replication of intracellular pathogens^{68,69}.

CD11c⁺ cells from BA.1 infected K18-hACE2 also produce high levels of IL-17 and IL-22 during LPS restimulation, with little or no change during in vivo B.1.351 infection. Both IL-17 and IL-22 play a significant roles in maintaining mucosal immunity via neutrophil recruitment to the infection site, up-production of antimicrobial proteins, and repair of the mucosal epithelial cell layer⁷⁰.

The differences and similarities between the CD11c⁺ cells from BA.1 exposed mice from different genetic backgrounds were also observed in the gene expression data. CD11c⁺ cells were classified as M-1 macrophages after gene enrichment classification. However, while genetic profiles from 129S1 CD11c⁺ cells are like those of other innate immune cells such as osteoclasts, microglia, and RAW cells, K18-hACE2 cellular transcriptomes were more indicative of adaptive immune response components such as follicular B-cells, b220⁺ B-cells and CD8⁺ T-cells. Of note, no gene counts for surface markers CD3e, CD4, CD8a, CD16 were found in any sample and the majority of B and T cells would have been removed by positive selection of CD11c⁺ cells, unless they would express (low levels of) CD11c.

Our findings support the previous finding that alveolar macrophages can be considered as a source of the “primary and altered cytokine” storm induced by SARS-CoV-2 infection^{46,71}. Our findings also show that different genetic backgrounds affect the immune phenotype of virus-exposed innate immune cells, which may either be beneficial or deleterious during re- or secondary infection, and provides a starting point to explore underlying genetic differences that can affect the host response to secondary SARS-CoV-2 infection in mouse models.

Methods

Cells and viruses

Vero-TMPRSS2 cells (BPS Bioscience, Cat# 78081) were cultured at 37 °C in 1X DMEM (Dulbecco’s modified Eagle medium) supplemented with 10% FBS (fetal bovine serum), 100 U/mL penicillin-streptomycin and 5 μ g/ml puromycin. hCoV-19/USA/NY-MSHSPSP-PV44476/2021 (GISAID: EPI_ISL_7908052) B.1.1.529 (Omicron, BA.1) and hCoV-19/USA/MD-HP01542/2021 JHU (Beta, B.1.351, a kind gift from Dr. Andrew Pekosz) cultured and tittered in Vero-TMPRSS2 cells followed by next-generation sequencing to confirm the stability of the variant specific mutations and the absence of undesired mutations.150 (plaque forming units) PFU of the H1N1 virus (NC99, A/New Caledonia/20/99) were injected into the allantoic fluid of 8-days old embryonated chicken eggs and was incubated for 48 h at 37 °C followed by an overnight incubation at 4 °C. The allantoic fluid, containing the virus, was carefully collected, briefly centrifuged, aliquoted, titrated and stored at –80 °C.

Animal experiments

All animal experiments were approved by the Institutional Biosafety committee and by the Institutional Animal Care and Use Committee at Icahn School of Medicine at Mount Sinai (ISMMS) (PROTO202100007). All SARS-CoV-2 virus experiments were performed in a biosafety level 3 facility at the ISMMS.

Heterozygous K18-hACE2 C57BL/6J (strain 2B6.Cg-Tg(K18-ACE2) 2Prln/J) and 129S1 (strain 129S1/SvImJ) female mice were procured from The Jackson Laboratory. The mice were housed in an animal vivarium at ISMMS with a 12-hour light-dark cycle and fed standard chow diet. Mice were transferred to the Animal biosafety level 3 facility one week prior to any virus inoculation experiments. In a first infection experiment, 3-month-old female K18-hACE2 and 129S1 mice were

anaesthetized with an intraperitoneal (IP) injection of a Ketamine/Xylazine cocktail and intranasally (IN) inoculated with either 10⁴ PFU (plaque forming unit) of B.1.1.529 (BA.1), 10² PFU of H1N1 virus (NC99) or mock media (PBS) in 50 μ L. At 7 and 30 days post infection (DPI), serum samples, BALF or whole lungs were collected from mice inoculated IN with either BA.1, NC99 or mock For the reinfection or secondary infection, the remaining mice were inoculated (IN) with 10⁴ PFU of B.1.351 or mock media 31 days after the first infection, resulting into 4 groups: Mock: Mock (1st infection mock and 2nd infection mock), Mock: B.1.351 (1st infection mock and 2nd infection B.1.351), BA.1: B.1.351 (1st infection BA.1 and 2nd infection B.1.351), and NC99: B.1.351. 4 days after the second infection all mice were euthanized by lethal pentobarbital IP injection (Fig. 1).

T-cell depletion experiments were carried out with Mock and BA.1 challenged mice that were infected at 30 days post infection with B.1.351, as described above. In these experiments, 72 h and 24 h prior to the B.1.351 reinfection, CD4⁺ and CD8⁺ T-cells were depleted in half of the animals via intraperitoneal injection of 500 μ g of CD4 (clone YTS 177, BioXCell) and 250 μ g of CD8 (clone 53-5.8, BioXCell) depleting antibodies diluted in PBS to a final volume of 200 μ L. After B.1.351, all experiments were performed as described above. Efficiency of T cell depletion was tested at 4 DPI using blood to stain for CD4⁺ and CD8⁺ T cells (Supplementary Fig. 2B). A T cell population (CD3⁺) was present at 4 DPI which stained with lower mean fluorescence intensity compared to the original CD4⁺ T cell population. This suggests that CD4⁺ T cell depletion was not as successful as CD8⁺ T cell depletion or the CD4⁺ T cell levels were going up already after being depleted.

For passive immunization, five 3-months-old female 129S1 mice were IP injected (150 μ L/mouse) with sera collected either from mock or BA.1 infected 129S1 mice from the first infection. After 12hrs, mice were IN inoculated with 10⁴ PFU of B.1.351 under Ketamine/Xylazine cocktail anesthesia. At 4 DPI all mice were euthanized by lethal pentobarbital IP injection [Fig. 1].

In experiments where lungs were collected, the cranial and middle lobes of the right lung from mice were collected and homogenized in 500 μ L of Phosphate Buffered Saline (PBS) and used for lung viral titers and cytokine profiling, whereas left lobe of the lungs was perfused and stored with 10% neutral buffered formalin for histology.

Humoral immune response against BA.1 or B.1.351 spike protein

ELISA against BA.1 or B.1.351 spike was performed on serum collected at 30 DPI. Nunc maxisorp 96-plates were coated with 0.1 μ g/well (in 50 μ L) of BA.1 (Sino Biologicals) or B.1.351 spike protein (Sino Biologicals) and incubated overnight at 4 °C using PBS as coating buffer. The next day, plates were washed three times with PBS-Tween20 (0.1%) (PBST) and blocked for 2 h with 2% BSA in PBST at room temperature, followed by three washes with PBST. 100 μ L of three-fold diluted serum starting from 1:10 were added into the wells and incubated for 2hrs at room temperature on a shaker. After three washes with PBST, 100 μ L of anti-mouse IgG HRP (Horse Radish Peroxidase) secondary antibodies were added in to the well and incubated for 1 h at room temperature on a shaker. Plates were washed three times with PBST, and a peroxidase reaction was catalyzed using 1-Step™ TMB (tetramethyl benzidine) ELISA Substrate Solutions (ThermoFisher Scientific) and incubated for 15 min at room temperature in the dark. Finally, the reaction was stopped by adding 50 μ L/well of ELISA Stop Solution (ThermoFisher Scientific). The optical density (OD) readings at 450 nm were obtained using a spectrophotometer.

Flow cytometry

For T-cell analysis, whole lungs collected at 30 DPI were dissociated into a single cell suspension using gentleMACS™ Octo Dissociator (Miltenyi Biotec) and Mouse Lung Dissociation Kit, mouse (Miltenyi Biotec) as per manufacturer’s instructions. The single cell suspension was then treated with eBioscience™ IX RBC Lysis Buffer (ThermoFisher

Scientific) to remove erythrocytes. The treated cells were then washed twice with PBS and resuspended in eBioscience™ Flow Cytometry Staining Buffer (ThermoFisher Scientific) containing 1:50 Mouse BD Fc Block™ (BD biosciences) antibody and incubated at room temperature for 15 min, followed by staining for viability-e780 (Fixable Viability Dye, eBioscience) and with 1 μ L of each antibody: anti-CD3-FITC (Clone 145-2C11, BD Bioscience), CD8a-PerCP (Clone 53-6.7, BD Bioscience), CD44-PE-CF549 (Clone 1M7, BD Bioscience), CD69-PE-Cy7 (HL2F3, BioLegend), CD103-APC antibodies (Clone M290, BD biosciences) and SARS-CoV-2 spike tetramer (VNFNFGN-PE, NIH core tetramer) for 15 min at room temperature in the dark. The cells were washed twice with eBioscience™ Flow Cytometry Staining Buffer (ThermoFisher Scientific) and fixed by adding 10% formaldehyde (5% final concentration in staining buffer) and incubating for 48 h at 4 °C. Fixed cells were washed twice with staining buffer and filtered through a 100 μ m cell strainer (Falcon) to remove clumped cells. Filtered single cell suspensions were then analyzed using the Gallios Flow Cytometer (Beckman Coulter) and FlowJo software. A representative gating scheme is provided as Supplementary Fig. 3.

To confirm successful of T-cell depletion, 200 μ L of blood was collected by terminal bleeding 4 days after the B.1.351 challenge into tubes containing 50 μ L of EDTA 0.5M (Invitrogen). RBC lysis, washes and Fc Block were performed as described above. Staining was performed with viability stain-eFluor520 (Fixable Viability Dye, eBioscience) and 1 μ L of each antibody: anti-CD3-BV480 (Clone 145-2C11, BD Bioscience), CD4-BV750 (Clone RM4-5, BD Bioscience) and CD8a-BB700 (Clone 53-6.7, BD Bioscience) antibodies and incubated for 30 mins at 4 °C. Cells were then fixed as described above and prepared for analysis in the cytometer. Analysis was performed in a using spectral flow Cytometer (Northern Lights, Cytek) and subsequent analysis and representation was performed with FlowJo software. We could confirm complete CD8+ T cell depletion until 4 DPI, the end of the experiment. At this time point, a population of CD4+ T cells started to reappear, be it with lower mean fluorescence intensity staining than the original CD4+ T cell population (Supplementary Fig. 2B).

Characterization of the CD11c+ alveolar compartment was performed using bronchoalveolar lavage fluid obtained from mice 7 and 30 DPI. A total of 1.2 mL of cold PBS-EDTA was used for the lavage, performed in two separate 600 μ L lavages. RBC lysis, washes and Fc Block were performed as described above. Staining was performed with 0.5 μ L of viability dye-eFluor520 (Fixable Viability Dye, eBioscience), 1 μ L of anti-CD45-PE-CF594 (Clone 30F-11, BD Biosciences), 1 μ L of CD3-AF532 (Clone 17A2, eBioscience) 0.5 μ L of CD11b-BV570 (Clone M1/70, BioLegend), 1.25 μ L Ly6C-BV510 (Clone HKL4, BioLegend), 1 μ L of CD11c-eFluor450 (Clone N418, eBioscience), 1 μ L of Ly6G-BV450 (Clone 1A8-Ly6g, eBioscience), 0.5 μ L of MHCII-PerCP (Clone M5/114.15.2, BioLegend), 2 μ L of B220-BV605 (Clone RA3-6B2, BioLegend) and 1 μ L of SiglecF-BV786 (Clone E50-2440, BD bioscience) antibodies and incubated for 30 min at 4 °C. Cells were then fixed as described above and prepared for analysis in the cytometer. Analysis was performed using spectral flow cytometry (Northern Lights, Cytek) and subsequent analysis and representation was performed with FlowJo software (v10.0.0), using the Downsample (v3.3.1), FlowSOM (v4.1.0) and UMAP_R (v4.0.4) plugins. A representative gating scheme is provided in Supplementary Fig. 4.

BALF CD11c+ cell analysis

CD11c+ cells were enriched from all groups ($n=5$ /group) at 30 DPI using CD11c MicroBeads UltraPure (Miltenyi Biotec) as per manufacturer's instructions. The pooled enriched cells were washed twice with cold RPMI-1640 medium containing 1X penicillin-streptomycin cocktail (Corning). Washed cells were plated in flat-bottom tissue culture 96-well plate (Falcon) at 200,000 cells/well. The cells were stimulated either with RPMI medium or with LPS (10 ng/ml) or with 10⁴ PFU of B.1.351 SARS-CoV-2 live virus for 48hrs. After 48hrs, cell

supernatants were collected, UV-inactivated, and used for cytokine profiling by Luminex multiplex ELISA.

Determination of viral titers in lungs

The cranial and middle lobes of the right lung lobes from both 129S1 and K18-hACE2 mice (mock: mock or mock: B.1.351 or BA.1: B.1.351 infected) were collected at 4 DPI and homogenized in sterile PBS. Homogenized lungs samples were cleared by centrifugation at 5000 g for 5 min at 4 °C and subjected to plaque assays¹¹. Briefly, twelve-well tissue culture plates were seeded with 1 \times 10⁶ Vero-TMPRSS2 cells per well. The following day, medium was removed and inoculated with 200 μ L of cleared lung homogenates serially diluted PBS. After 1 hr, the inoculum was removed and replaced with 1% Oxoid™ Purified Agar (ThermoFisher Scientific) in 1xDMEM + 2% FBS overlay. Plates were incubated for 72 h at 37 °C supplemented with 5% CO₂, and then fixed with 5% paraformaldehyde (final concentration) in PBS overnight at 4 °C. The 5% paraformaldehyde and agar overlay were carefully removed, and plates were washed once with PBST. Plates were immuno-stained using 1:1000 anti-SARS-CoV-2-N monoclonal antibody (1C7C7) on a shaker at room temperature for 1 h followed by 1:5000 anti-mouse IgG HRP-conjugated antibody (ThermoFisher Scientific) incubated at room temperature for 1 h. The peroxidase reaction was catalyzed using KPL TrueBlue Peroxidase Substrate (Seracare) for 15 min at room temperature and washed with tap water. The immuno-stained plaques were counted, and titers were calculated and represented as PFU/mL.

Cytokines and chemokines multiplex analysis

The cranial and middle lobes of the right lungs from both 129S1 and K18-hACE2 mice K18-hACE2 mice (mock: mock or mock: B.1.351 or BA.1:B.1.351 infected) were collected at 4 DPI, homogenized. Homogenized lungs samples were centrifuged at 5000 \times g for 5 min at 4 °C and transferred into clear- U-bottom 96-well plate (Falcon). Samples were inactivated with ultraviolet (UV-C) light for 15 mins on ice. Inactivated samples were then used to profile cytokine and chemokine levels using a mouse 26-plex, bead-based Luminex assay (catalogue number EPXR260-26088-901). The assay was performed according to the manufacturer's instructions, and all incubation steps occurred on an orbital shaker set at 300 rpm. Briefly, 50 μ L of clarified lung homogenate supernatant was combined with beads in a lidded, black 96-well plate supplied as part of the kit and incubated for 30 min at room temperature, and then overnight at 4 °C. The next day, the plate was allowed to equilibrate to room temperature for 30 min, washed 3 times with 150 μ L per well of 1 \times wash buffer, and then 25 μ L per well of 1 \times detection antibody mixture was added for 30 min at room temperature. The plate was washed 3 times, and then 50 μ L per well of 1 \times Streptavidin-PE solution was added for 30 min at room temperature. After washing 3 times, 120 μ L per well of reading buffer was added, and the plate was incubated for 5 min at room temperature. Data were acquired on a Luminex 100/200 analyzer (Millipore) with xPONENT software (version 4.3) and analyzed using GraphPad Prism (version 10.0) and R (version 4.0.5).

Pathology

The left lobe of the lungs was perfused and fixed in 10% formaldehyde in PBS. After 4 weeks, 10% formaldehyde was replaced with 1X PBS and shipped to Wyoming State Veterinary Laboratory (Laramie, WY) for tissue processing and histology examination. The H&E-stained slides were blindly scored by a Board-Certified Veterinary Pathologist. Lung tissue sections were scored as per Table 1.

Long read transcriptome profiling

The pooled enriched cells were also used for transcriptome profiling of CD11c+ cells. The RNA from enriched cells was isolated using Trizol, and mRNA was enriched using Next Poly (A) mRNA Magnetic Isolation

Table 1 | Scoring matrix for the histology examination

Score	Area affected	Epithelial degeneration/necrosis	Inflammation
0	none	None	None
1	5–10%	Minimal; scattered cell necrosis/vacuolation affecting 5 to 10% of tissue section	Minimal; scattered inflammatory cells affecting 5–10% of tissue section
2	10–25%	Mild; scattered cell necrosis/vacuolation	Multifocal, few inflammatory cells
3	25–50%	Moderate; multifocal vacuolation or sloughed/necrotic cells	Thin layer of cells (<5 cell layer thick)
4	50–75%	Marked; multifocal/segmental necrosis, epithelial loss/effacement	Thick layer of cells (>5 cell layer thick)
5	>75%	Severe; coalescing areas of necrosis, parenchymal effacement	Confluent areas of inflammation

Module (NEB) as per manufacturer's instructions. One nanogram of purified mRNA then used to prepare cDNA library using PCR-cDNA Sequencing Kit (Oxford Nanopore) as per manufacturers' instructions. RNA sequencing was then performed on the MinION MK1b device (Oxford Nanopore) using FLO-MINI06D Flow cells (Oxford Nanopore).

The output reads were analyzed using Minimap2, Samtools, and Stringtie packages^{72–74}. The normalized final counts then were analyzed and visualized using R packages (ggsankey) and Graphpad Prism⁷⁵.

Other statistical analysis

Unpaired t-tests, Mann–Whitney U test, Ordinary one-way ANOVA with Dunnett's multiple comparison test or Kruskal–Wallis test with Dunnett's multiple comparison test were used, when appropriate, to determine the Statistical significance between experimental groups, where *p*-values > 0.05 are not represented, smaller *p*-values are represented by exact values. The number of technical replicates and statistical test performed are specified in each case.

Availability of biological materials

Unique biological materials generated for the work presented in this manuscript are available upon request for research purposes and will be shared according to standard material transfer agreements between research institutes. Requests for a material transfer agreement (MTA) can be addressed to Michael Schotsaert at Michael.Schotsaert@mssm.edu.

Reporting summary

Further information on research design is available in the Nature Portfolio Reporting Summary linked to this article.

Data availability

The sequencing data generated in this study have been deposited in the Gene Expression Omnibus database under accession code [GSE248984](https://www.ncbi.nlm.nih.gov/geo/query/acc.cgi?acc=GSE248984). The remaining data generated in this study are provided in the Manuscript, Supplementary Information and Source Data file. Source data are provided with this paper.

References

- Markov, P. V. et al. The evolution of SARS-CoV-2. *Nat. Rev. Microbiol.* **21**, 361–379 (2023).
- Abu-Raddad, L. J. et al. Assessment of the Risk of Severe Acute Respiratory Syndrome Coronavirus 2 (SARS-CoV-2) Reinfection in an Intense Reexposure Setting. *Clin. Infect. Dis.* **73**, e1830–e1840 (2021).
- Babiker, A., Marvil, C. E., Waggoner, J. J., Collins, M. H. & Piantadosi, A. The Importance and Challenges of Identifying SARS-CoV-2 Reinfections. *J. Clin. Microbiol.* **59**, <https://doi.org/10.1128/jcm.02769-20> (2021).
- Nguyen, N. N. et al. SARS-CoV-2 reinfection and COVID-19 severity. *Emerg. Microbes Infect.* **11**, 894–901 (2022).
- Stein, C. et al. Past SARS-CoV-2 infection protection against re-infection: a systematic review and meta-analysis. *Lancet* **401**, 833–842 (2023).
- Hwang, J. H. et al. Influenza viral infection is a risk factor for severe illness in COVID-19 patients: a nationwide population-based cohort study. *Emerg. Microbes Infect.* **12**, 2164215 (2023).
- Russell, C. D., Lone, N. I. & Baillie, J. K. Comorbidities, multi-morbidity and COVID-19. *Nat. Med.* **29**, 334–343 (2023).
- Ng, W. H. et al. Comorbidities in SARS-CoV-2 Patients: a Systematic Review and Meta-Analysis. *mBio* **12**, e03647-20 (2021).
- Andreaskos, E. et al. A global effort to dissect the human genetic basis of resistance to SARS-CoV-2 infection. *Nat. Immunol.* **23**, 159–164 (2022).
- Ovsyannikova, I. G., Haralambieva, I. H., Crooke, S. N., Poland, G. A. & Kennedy, R. B. The role of host genetics in the immune response to SARS-CoV-2 and COVID-19 susceptibility and severity. *Immunol. Rev.* **296**, 205–219 (2020).
- Diego, J. G.-B. et al. Breakthrough infections by SARS-CoV-2 variants boost cross-reactive hybrid immune responses in mRNA-vaccinated Golden Syrian Hamsters. *PLoS Pathog.* **20**, e1011805 (2024).
- Flacco, M. E. et al. Risk of reinfection and disease after SARS-CoV-2 primary infection: Meta-analysis. *Eur. J. Clin. Invest.* **52**, e13845 (2022).
- Medić, S. et al. Risk and severity of SARS-CoV-2 reinfections during 2020–2022 in Vojvodina, Serbia: A population-level observational study. *Lancet Reg. Health Eur.* **20**, 100453 (2022).
- Pulliam, J. R. C. et al. Increased risk of SARS-CoV-2 reinfection associated with emergence of Omicron in South Africa. *Science* **376**, eabn4947 (2022).
- O Murchu, E. et al. Quantifying the risk of SARS-CoV-2 reinfection over time. *Rev. Med. Virol.* **32**, e2260 (2022).
- Kellam, P. & Barclay, W. The dynamics of humoral immune responses following SARS-CoV-2 infection and the potential for reinfection. *J. Gen. Virol.* **101**, 791–797 (2020).
- Muñoz-Fontela, C. et al. Animal models for COVID-19. *Nature* **586**, 509–515 (2020).
- Halfmann, P. J. et al. SARS-CoV-2 Omicron virus causes attenuated disease in mice and hamsters. *Nature*. **603**, 687–692 (2022).
- Rathnasinghe R. et al. Characterization of SARS-CoV-2 Spike mutations important for infection of mice and escape from human immune sera. *Nat. Commun* **13**, 3921 (2022).
- Gretebeck, L. M. & Subbarao, K. Animal models for SARS and MERS coronaviruses. *Curr. Opin. Virol.* **13**, 123–129 (2015).
- Singh, A. et al. A Comprehensive Review of Animal Models for Coronaviruses: SARS-CoV-2, SARS-CoV, and MERS-CoV. *Virol. Sin.* **35**, 290–304 (2020).
- Saravanan, U. B., Namachivayam, M., Jeewon, R., Huang, J.-D. & Durairajan, S. S. K. Animal models for SARS-CoV-2 and SARS-CoV-1 pathogenesis, transmission and therapeutic evaluation. *World J. Virol.* **11**, 40–56 (2022).
- Venkataraman, T., Coleman, C. M. & Frieman, M. B. Overactive Epidermal Growth Factor Receptor Signaling Leads to Increased Fibrosis after Severe Acute Respiratory Syndrome Coronavirus Infection. *J. Virol.* **91**, e00182-17 (2017).
- Wang, T. et al. Influenza-trained mucosal-resident alveolar macrophages confer long-term antitumor immunity in the lungs. *Nat. Immunol.* **24**, 423–438 (2023).

25. Iliakis, C. S. et al. The role of recruitment versus training in influenza-induced lasting changes to alveolar macrophage function. *Nat. Immunol.* **24**, 1639–1641 (2023).
26. Hua, X. et al. Nasal priming by a murine coronavirus provides protective immunity against lethal heterologous virus pneumonia. *JCI Insight* **3**, e99025 (2018).
27. Xiong, H. et al. A flexible estimating equations approach for mapping function-valued traits. *Genetics* **189**, 305–316 (2011).
28. Ackert-Bicknell, C. L. et al. Mouse BMD quantitative trait loci show improved concordance with human genome-wide association loci when recalculated on a new, common mouse genetic map. *J. Bone Miner. Res. J. Am. Soc. Bone Miner. Res.* **25**, 1808–1820 (2010).
29. Chesler, E. J. et al. Quantitative trait loci for sensitivity to ethanol intoxication in a C57BL/6J×129S1/SvImJ inbred mouse cross. *Mamm. Genome. J. Int. Mamm. Genome Soc.* **23**, 305–321 (2012).
30. Ishimori, N. et al. Quantitative trait loci that determine plasma lipids and obesity in C57BL/6J and 129S1/SvImJ inbred mice. *J. Lipid Res.* **45**, 1624–1632 (2004).
31. Whitehead, G. S., Walker, J. K. L., Berman, K. G., Foster, W. M. & Schwartz, D. A. Allergen-induced airway disease is mouse strain dependent. *Am. J. Physiol. -Lung Cell. Mol. Physiol.* **285**, L32–L42 (2003).
32. Clough, B. et al. C57BL/6 and 129 inbred mouse strains... *Wellcome Open Res.* **4**, 124 (2019).
33. Krapp, C. et al. Guanylate Binding Protein (GBP) 5 Is an Interferon-Inducible Inhibitor of HIV-1 Infectivity. *Cell Host Microbe* **19**, 504–514 (2016).
34. Braun, E. et al. Guanylate-Binding Proteins 2 and 5 Exert Broad Antiviral Activity by Inhibiting Furin-Mediated Processing of Viral Envelope Proteins. *Cell Rep.* **27**, 2092–2104.e10 (2019).
35. Nordmann, A., Wixler, L., Boergeling, Y., Wixler, V. & Ludwig, S. A new splice variant of the human guanylate-binding protein 3 mediates anti-influenza activity through inhibition of viral transcription and replication. *FASEB J.* **26**, 1290–1300 (2012).
36. Kandeel, M. & El-Deeb, W. Omicron variant receptor-binding domain phylogenetics and molecular dynamics. *Comput. Biol. Med.* **146**, 105633 (2022).
37. Gupta, G. et al. Th1/Th2/Th17 Cytokine Profile among Different Stages of COVID-19 Infection. *Natl Acad. Sci. Lett.* **45**, 363–369 (2022).
38. Ling, L. et al. Longitudinal Cytokine Profile in Patients With Mild to Critical COVID-19. *Front. Immunol.* **12**, 763292 (2021).
39. Han, H. et al. Profiling serum cytokines in COVID-19 patients reveals IL-6 and IL-10 are disease severity predictors. *Emerg. Microbes Infect.* **9**, 1123–1130 (2020).
40. Queiroz, M. A. F. et al. Cytokine Profiles Associated With Acute COVID-19 and Long COVID-19 Syndrome. *Front. Cell. Infect. Microbiol.* **12**, 922422 (2022).
41. Qin, C. et al. Dysregulation of Immune Response in Patients With Coronavirus 2019 (COVID-19) in Wuhan, China. *Clin. Infect. Dis.* **71**, 762–768 (2020).
42. Ghazavi, A., Ganji, A., Keshavarzian, N., Rabiemajd, S. & Mosayebi, G. Cytokine profile and disease severity in patients with COVID-19. *Cytokine* **137**, 155323 (2021).
43. Davidson, S., Crotta, S., McCabe, T. M. & Wack, A. Pathogenic potential of interferon $\alpha\beta$ in acute influenza infection. *Nat. Commun.* **5**, 3864 (2014).
44. Bégin, P. et al. Convalescent plasma for hospitalized patients with COVID-19: an open-label, randomized controlled trial. *Nat. Med.* **27**, 2012–2024 (2021).
45. Azkur, A. K. et al. Immune response to SARS-CoV-2 and mechanisms of immunopathological changes in COVID-19. *Allergy* **75**, 1564–1581 (2020).
46. Dentone, C. et al. Bronchoalveolar lavage fluid characteristics and outcomes of invasively mechanically ventilated patients with COVID-19 pneumonia in Genoa, Italy. *BMC Infect. Dis.* **21**, 353 (2021).
47. Netea, M. G. et al. Defining trained immunity and its role in health and disease. *Nat. Rev. Immunol.* **20**, 375–388 (2020).
48. Ochando, J., Mulder, W. J. M., Madsen, J. C., Netea, M. G. & Duijvenvoorden, R. Trained immunity — basic concepts and contributions to immunopathology. *Nat. Rev. Nephrol.* **19**, 23–37 (2023).
49. Aegerter, H. et al. Influenza-induced monocyte-derived alveolar macrophages confer prolonged antibacterial protection. *Nat. Immunol.* **21**, 145–157 (2020).
50. George, L. & Brightling, C. E. Eosinophilic airway inflammation: role in asthma and chronic obstructive pulmonary disease. *Ther. Adv. Chronic Dis.* **7**, 34–51 (2016).
51. Eltboli, O. et al. COPD exacerbation severity and frequency is associated with impaired macrophage efferocytosis of eosinophils. *BMC Pulm. Med.* **14**, 112 (2014).
52. Kulkarni, N. S. et al. Eosinophil protein in airway macrophages: A novel biomarker of eosinophilic inflammation in patients with asthma. *J. Allergy Clin. Immunol.* **126**, 61–69.e3 (2010).
53. Felton, J. M. et al. Mer-mediated eosinophil efferocytosis regulates resolution of allergic airway inflammation. *J. Allergy Clin. Immunol.* **142**, 1884–1893.e6 (2018).
54. Mishra, A. & Rothenberg, M. E. Intratracheal IL-13 induces eosinophilic esophagitis by an IL-5, eotaxin-1, and STAT6-dependent mechanism. *Gastroenterology* **125**, 1419–1427 (2003).
55. Fulkerson, P. C., Fischetti, C. A., Hassman, L. M., Nikolaidis, N. M. & Rothenberg, M. E. Persistent Effects Induced by IL-13 in the Lung. *Am. J. Respir. Cell Mol. Biol.* **35**, 337–346 (2006).
56. Zhu, Z. et al. Pulmonary expression of interleukin-13 causes inflammation, mucus hypersecretion, subepithelial fibrosis, physiologic abnormalities, and eotaxin production. *J. Clin. Invest.* **103**, 779–788 (1999).
57. Gieseck, R. L., Wilson, M. S. & Wynn, T. A. Type 2 immunity in tissue repair and fibrosis. *Nat. Rev. Immunol.* **18**, 62–76 (2018).
58. Madala, S. K. et al. Matrix Metalloproteinase 12-Deficiency Augments Extracellular Matrix Degrading Metalloproteinases and Attenuates IL-13-Dependent Fibrosis. *J. Immunol.* **184**, 3955–3963 (2010).
59. Mommert, S., Ratz, L., Stark, H., Gutzmer, R. & Werfel, T. The histamine H4 receptor modulates the differentiation process of human monocyte-derived M1 macrophages and the release of CCL4/MIP-1 β from fully differentiated M1 macrophages. *Inflamm. Res.* **67**, 503–513 (2018).
60. Kawano, H. et al. IL-10-producing lung interstitial macrophages prevent neutrophilic asthma. *Int. Immunol.* **28**, 489–501 (2016).
61. Yang, X., Wang, S., Fan, Y. & Han, X. IL-10 deficiency prevents IL-5 overproduction and eosinophilic inflammation in a murine model of asthma-like reaction. *Eur. J. Immunol.* **30**, 382–391 (2000).
62. Lauw, F. N. et al. Proinflammatory Effects of IL-10 During Human Endotoxemia. *J. Immunol.* **165**, 2783–2789 (2000).
63. Tilg, H. et al. Treatment of Crohn's disease with recombinant human interleukin 10 induces the proinflammatory cytokine interferon γ . *Gut* **50**, 191–195 (2002).
64. Lee, C. G. et al. Transgenic Overexpression of Interleukin (IL)-10 in the Lung Causes Mucus Metaplasia, Tissue Inflammation, and Airway Remodeling via IL-13-dependent and -independent Pathways*. *J. Biol. Chem.* **277**, 35466–35474 (2002).
65. Crapster-Pregont, M., Yeo, J., Sanchez, R. L. & Kuperman, D. A. Dendritic cells and alveolar macrophages mediate IL-13-induced airway inflammation and chemokine production. *J. Allergy Clin. Immunol.* **129**, 1621–7.e3 (2012).
66. Ford, J. G. et al. IL-13 and IFN- γ : Interactions in Lung Inflammation. *J. Immunol.* **167**, 1769–1777 (2001).

67. Varma, T. K., Lin, C. Y., Toliver-Kinsky, T. E. & Sherwood, E. R. Endotoxin-Induced Gamma Interferon Production: Contributing Cell Types and Key Regulatory Factors. *Clin. Diagn. Lab. Immunol.* **9**, 530–543 (2002).
68. Luo, X. et al. Brucella Downregulates Tumor Necrosis Factor- α to Promote Intracellular Survival via Omp25 Regulation of Different MicroRNAs in Porcine and Murine Macrophages. *Front. Immunol.* **8**, 2013 (2018).
69. Adler, H. et al. Cytokine regulation by virus infection: bovine viral diarrhoea virus, a flavivirus, downregulates production of tumor necrosis factor alpha in macrophages in vitro. *J. Virol.* **70**, 2650–2653 (1996).
70. Valeri, M. & Raffatellu, M. Cytokines IL-17 and IL-22 in the host response to infection. *Pathog. Dis.* **74**, ftw111 (2016).
71. Shimabukuro-Vornhagen, A. et al. Cytokine release syndrome. *J. Immunother. Cancer* **6**, 56 (2018).
72. Li, H. New strategies to improve minimap2 alignment accuracy. *Bioinformatics* **37**, 4572–4574 (2021).
73. Danecek, P. et al. Twelve years of SAMtools and BCFtools. *Giga-Science* **10**, giab008 (2021).
74. Kovaka, S. et al. Transcriptome assembly from long-read RNA-seq alignments with StringTie2. *Genome Biol.* **20**, 278 (2019).
75. [davidsjoberg/ggsankey](https://github.com/davidsjoberg/ggsankey): Sankey, Alluvial and Sankey Bump Plots version 0.0.99999 from GitHub. <https://rdr.io/github/davidsjoberg/ggsankey/>.

Acknowledgements

We thank Daniel Flores, Marlene Espinoza, Jane Deng, and Ryan Camping for excellent administrative support, Richard Cadagan, Leonie Gruneberg and Farah El-Ayache for technical support and Randy Albrecht for management and organization of the BSL3 facility. SARS-CoV-2 work in the M.S. laboratory is supported by NIH/NIAID R01AI160706 and NIH/NIDDK R01DK130425. L.A.C. received support through a Public Health Service Institutional Research T32 Training Award (AI07647). This study was also partly funded by CRIPT (Center for Research on Influenza Pathogenesis and Transmission), a NIH NIAID funded Center of Excellence for Influenza Research and Response (CEIRR, contract number 75N93021C00014), and by NIAID contract 75N93019C00046 and U19AI135972 to AG-S.

Author contributions

G.S. and J.G.B.D. contributed equally to this manuscript. G.S., J.G.B.D., P.W., S.C.P., L.A.C., M.N., G.L., Y.B., M.P., V.Y., S.C.C., B.W. and M.S. designed and/or performed experiments. G.S., J.G.B.D., L.A.C., M.N., G.L., S.S., S.C.C., B.W., and M.S. analyzed data. G.S., J.G.B.D., P.W., A.G.S., S.C.C. generated critical reagents. S.C.C. and M.S. oversaw the conception and design of the experiments. L.P. submitted and curated data. G.S., J.G.B.D., S.C.C., and M.S. wrote the manuscript or substantially revised it.

Competing interests

The M.S. laboratory has received unrelated funding support in sponsored research agreements from Phio Pharmaceuticals, 7Hills Pharma,

ArgenX BV and Moderna. The A.G.-S. laboratory has received research support from GSK, Pfizer, Senhwa Biosciences, Kenall Manufacturing, Blade Therapeutics, Avimex, Johnson & Johnson, Dynavax, 7Hills Pharma, Pharmamar, ImmunityBio, Accurius, Nanocomposix, Hexamer, N-fold LLC, Model Medicines, Atea Pharma, Applied Biological Laboratories and Merck, outside of the reported work. A.G.-S. has consulting agreements for the following companies involving cash and/or stock: Castlevax, Amovir, Vivaldi Biosciences, Contrafact, 7Hills Pharma, Avimex, Pagoda, Accurius, Esperovax, Farmak, Applied Biological Laboratories, Pharmamar, CureLab Oncology, CureLab Veterinary, Synairgen, Paratus and Pfizer, outside of the reported work. A.G.-S. has been an invited speaker in meeting events organized by Seqirus, Janssen, Abbott and Astrazeneca. A.G.-S. is inventor on patents and patent applications on the use of antivirals and vaccines for the treatment and prevention of virus infections and cancer, owned by the Icahn School of Medicine at Mount Sinai, New York. The remaining authors declare no competing interests.

Additional information

Supplementary information The online version contains supplementary material available at <https://doi.org/10.1038/s41467-024-54334-7>.

Correspondence and requests for materials should be addressed to Michael Schotsaert.

Peer review information *Nature Communications* thanks the anonymous reviewers for their contribution to the peer review of this work. A peer review file is available.

Reprints and permissions information is available at <http://www.nature.com/reprints>

Publisher's note Springer Nature remains neutral with regard to jurisdictional claims in published maps and institutional affiliations.

Open Access This article is licensed under a Creative Commons Attribution-NonCommercial-NoDerivatives 4.0 International License, which permits any non-commercial use, sharing, distribution and reproduction in any medium or format, as long as you give appropriate credit to the original author(s) and the source, provide a link to the Creative Commons licence, and indicate if you modified the licensed material. You do not have permission under this licence to share adapted material derived from this article or parts of it. The images or other third party material in this article are included in the article's Creative Commons licence, unless indicated otherwise in a credit line to the material. If material is not included in the article's Creative Commons licence and your intended use is not permitted by statutory regulation or exceeds the permitted use, you will need to obtain permission directly from the copyright holder. To view a copy of this licence, visit <http://creativecommons.org/licenses/by-nc-nd/4.0/>.

© The Author(s) 2024